

Water Resources Research



RESEARCH ARTICLE

10.1029/2021WR031045

Key Points:

- A suspended sediment concentration (SSC) equation for turbulent flows is proposed and tested
- The equation is derived from a co-spectral budget that accounts for energy distribution in all eddy sizes
- The effects of Reynolds number and a scale-dependent Schmidt number on SSC are explicitly described

Correspondence to:

S. Li, shuolin.li@duke.edu

Citation:

Li, S., Bragg, A. D., & Katul, G. (2022). A co-spectral budget model links turbulent eddies to suspended sediment concentration in channel flows. *Water Resources Research*, 58, e2021WR031045. https://doi.org/10.1029/2021WR031045

Received 14 AUG 2021 Accepted 21 FEB 2022

Author Contributions:

Conceptualization: Shuolin Li, Andrew D. Bragg, Gabriel Katul

Data curation: Shuolin Li, Andrew D.

Bragg

Formal analysis: Shuolin Li Funding acquisition: Gabriel Katul Investigation: Shuolin Li, Andrew D. Brage

Methodology: Shuolin Li, Gabriel Katul Project Administration: Gabriel Katul

Resources: Shuolin Li Software: Shuolin Li

Supervision: Andrew D. Bragg, Gabriel Katul

Validation: Shuolin Li Visualization: Shuolin Li Writing – original draft: Shuolin Li Writing – review & editing: Shuolin Li, Andrew D. Bragg, Gabriel Katul

© 2022. American Geophysical Union. All Rights Reserved.

This is an open access article under the terms of the Creative Commons Attribution License, which permits use, distribution and reproduction in any medium, provided the original work is properly cited.

A Co-Spectral Budget Model Links Turbulent Eddies to Suspended Sediment Concentration in Channel Flows

Shuolin Li^{1,2} , Andrew D. Bragg¹ , and Gabriel Katul^{1,2}

¹Department of Civil and Environmental Engineering, Duke University, Durham, NC, USA, ²Nicholas School of the Environment, Duke University, Durham, NC, USA

Abstract The vertical distribution of suspended sediment concentration remains a subject of active research given its relevance to a plethora of problems in hydraulics, hydrology, ecology, and water quality control. Many of the classical theories developed over the course of 90 years represent the effects of turbulence on suspended sediments (SS) using an effective mixing length or eddy diffusivity without explicitly accounting for the energetics of turbulent eddies across scales. To address this gap, the turbulent flux of sediments is derived using a co-spectral budget (CSB) model that can be imminently used in SS and other fine particle transport models. The CSB closes the pressure-redistribution effect using a spectral linear Rotta scheme modified to include isotropization of production and interactions between turbulent eddies and sediment grains through a modified scale-dependent de-correlation time. The result is a formulation similar in complexity to the widely used Rouse's equation but with all characteristic scales, Reynolds number, and Schmidt number effects derived from well-established spectral shapes of the vertical velocity and accepted constants from turbulence models. Finally, the proposed CSB model can recover Prandtl's and Rouse's equations under restricted conditions.

1. Introduction

In his classic treatise on sediment transport, Hans Albert Einstein presented a definition of suspended sediments (SS) and the role of turbulence in maintaining suspension as follows (Einstein, 1950):

"The characteristic definition of a suspended solid particle is that its weight is supported by the surrounding fluid during its entire motion. While being moved by the fluid, the solid particle, which is heavier than the fluid, tends to settle in the surrounding fluid. If the fluid flow has only horizontal velocities, it is impossible to explain how any sediment particle can be permanently suspended. Only if the irregular motion of the fluid particles, called turbulence, is introduced can one show that sediment may be permanently suspended."

This operational definition of SS has become de facto standard in textbooks and research articles alike (Dey, 2014; Dey & Ali, 2020; Green & Coco, 2014). Despite some 80 years of research, the dominant factors controlling suspended sediment concentration (SSC) in streams continue to draw interest due to its multiple connections to ecosystem benefits and water quality degradation issues (Dai et al., 2016; Huai et al., 2019, 2020; Huai et al., 2021; Long & Pavelsky, 2013; Muste et al., 2005; Nazeer et al., 2014; Tseng & Tinoco, 2020). High SSC can intercept photosynthetically active radiation necessary for sustaining submerged aquatic plants in lakes and rivers. The presence of high SSC is also related to eutrophication and corollary water quality issues (Kellogg et al., 2014; Yujun et al., 2008), clogging of gills of fish and other aquatic organisms, and accelerating the denitrification process (Liu et al., 2013). In certain cases, sediments provide necessary nutrients to aquatic plants and are of primary significance to sustaining nearshore ecosystems such as floodplains and marshes. The role of SS in element-cycling has been highlighted in several studies (Lupker et al., 2011; Mohtar et al., 2020) as well. Another issue is the connection between SSC and micro/nano-plastics in saline environments. Recent work has shown that SS can promote polystyrene nano plastics settling in the presence of saline conditions, prompting further interest in SSC distribution in natural waters (Li, Katul, & Huai, 2019).

Even in the most idealized flow condition with a balance between the gravitational settling flux and the vertical turbulent sediment flux, the description of SSC remains a recalcitrant problem. A model for the turbulent vertical flux is required and is often derived using Reynolds' analogy (Dey, 2014) where eddies are assumed to transport momentum and SS similarly. This analogy was the cornerstone of the well-celebrated Rouse's

LIET AL.



formula (Rouse, 1939) that assumes sediment diffusivity is proportional to eddy viscosity. Since the early work of O'Brien (1933), Prandtl, and von Karman (1934), these analogies have spawned numerous theories and closure models for the mixing length (Bombardelli & Jha, 2009; Bombardelli & Moreno, 2012; Dey, 2014; Nie et al., 2017; Vanoni, 1984). However, these models make no explicit contact with turbulent eddies and their associated kinetic energy distribution in the vertical direction. It is precisely the vertical turbulent kinetic energy component in eddies of varying sizes that maintains sediments in suspension (Dey, 2014; Mazumder & Ghoshal, 2006; Scully & Friedrichs, 2003).

The turbulent vertical flux of SS is directly modeled in this work from the spectrum of turbulent eddies thereby providing a new perspective on Reynold's analogy, the multiple length scales involved in describing SSC, and the emergence of Reynolds, Rouse, Schmidt, and Stokes numbers when linking eddy viscosity with eddy diffusivity for SS. The role of the Reynolds number has been introduced in prior studies as a damping correction to the mixing length (Nezu & Azuma, 2004; Van Driest, 1956; Wallin & Johansson, 2000) whereas the Rouse number is operationally used in the classification of sediment load. The proposed approach uses a co-spectral budget model (CSB) derived from an approximated Navier-Stokes equation in spectral form for the Reynolds stress and SS turbulent flux. It uses a spectral Rotta scheme modified to include the isotropization of the production term for the pressure decorrelation effect (Katul et al., 2013) and a Schmidt number effect similar in form to van Rijin's bulk formulation (van Rijn, 1984) for linking the fluid and particle velocity decorrelation time scales, explicitly made here scale-dependent. The newly proposed formulation tested with several published experiments that span a wide range of flow conditions and grain properties (diameter and density). A comparison against the widely used Rouse formula is discussed with a focus on the conditions where the CSB recovers Rouses's formula.

2. Theory

2.1. Definitions and General Considerations

As a starting point to review models for SSC profiles in streams, a prismatic rectangular channel with constant width B and bed slope S_o is considered. The flow is assumed to be steady and uniform with constant water depth B and flow rate B. For small slopes, a balance between gravitational and frictional forces for a length segment B along the flow direction B yields

$$\rho(BH\Delta x)gS_o = 2\tau_s(H\Delta x) + \tau_o(B\Delta x),\tag{1}$$

where τ_s is the side stress, τ_o is the bed stress, g is the gravitational acceleration, and ρ is the fluid density. This expression can be re-arranged as

$$u_*^2 = \frac{\tau_o}{\rho} = gHS_o \left(1 + \frac{2H}{B} \frac{\tau_s}{\tau_o} \right)^{-1},$$
 (2)

where u_* is the friction (or shear) velocity. For the case where $\tau_s = \tau_o$, $u_*^2 = g R_h S_o$ with $R_h = H(1 + 2H/B)^{-1}$ being the hydraulic radius. When $H/B \ll 1$ (i.e., a wide-channel approximation), $R_h = H$ and the bed stress dominates the total frictional stress strictly based on a geometric consideration. In many SS laboratory experiments, the wide channel approximation may not hold with 2H/B being of order unity. However, in these experiments, the channel bed is covered with sediments whereas the channel sides remain smooth (plastic or glass) to permit optical access. This difference in roughness between sides and bed leads to $\tau_s/\tau_o \ll 1$. Hence, 2H/B may be of order unity in some experiments but $\tau_s/\tau_o \ll 1$ allowing $\tau_o/\rho \approx gHS_o$. Fully turbulent flow conditions are also assumed to prevail so that the bulk Reynolds number $Re_b = U_bH/\nu > 500$, where ν is the kinematic viscosity and U_b is the bulk or depth-averaged velocity given as

$$U_b = \frac{Q}{BH} \approx \frac{1}{H} \int_0^H \overline{u}(z) dz, \tag{3}$$

where $\overline{u}(z)$ is the mean velocity at vertical distance z from the channel bed (positive upwards), and overline indicates ensemble-averaging usually determined from time averaging. For such a flow, the Reynolds-averaged mean continuity equation for SSC in steady and planar homogeneous flow at high Re_b and small stokes number yields (Richter & Chamecki, 2018)

LI ET AL. 2 of 19

$$\frac{\partial \overline{C}(z)}{\partial t} = 0 = -\frac{\partial}{\partial z} \left[\overline{w'C'} - w_s \overline{C} \right] + S_e(z), \tag{4}$$

where t is time, $C = \overline{C} + C'$ is the instantaneous volumetric SSC in the flow, primed quantities are the fluctuating component, w is the instantaneous vertical velocity component with $\overline{w} = 0$ (assuming water is of constant ρ), $\overline{w'C'}$ is the turbulent vertical flux that requires a closure model, w_s is the terminal velocity of sediment grains, and $S_e(z)$ is the sediment source presumed to be situated in a thin region above the channel bed known as the emission layer. By restricting the analysis to a plane just above the emission layer (i.e., z = 0 is set just above the emission layer), $S_e(z) = 0$ throughout. The SSC mean continuity equation above also assumes that the instantaneous particle vertical advection velocity $w_p = w - w_s$ (i.e., imbalance between the fluid vertical velocity and w_s) thereby ignoring any particle inertial effects. In a regime where particle inertia is weak but finite, to a leading approximation, an inertial correction can be added and given by $w_p = w - w_s - \tau_p(Dw/Dt)$, where D(.)/Dt is the material derivative (local and advective) along a fluid particle trajectory, and $\tau_p = w_s/g$ is a particle time scale. Including these inertial effects in the mean SS particle continuity equation leads to (Ferry & Balachandar, 2001; Richter & Chamecki, 2018)

$$\left[\overline{w'C'} - w_s\overline{C}\right] - \Phi(z) = 0; \ \Phi(z) = \tau_p \left[\overline{C\frac{Dw'}{Dt}}\right] = \frac{1}{2}\tau_p \overline{C}\frac{\partial \sigma_w^2}{\partial z} + \tau_p \overline{\left[C'\frac{Dw'}{Dt}\right]}, \tag{5}$$

where $\sigma_w^2 = \overline{w'w'}$ is the fluid vertical velocity variance at z and $\Phi(z)$ is the sum of a turbophoretic effect that arises due to finite $\partial \sigma_w^2/\partial z$ in in-homogeneous flows such as channels (Johnson et al., 2020; Reeks, 1983; Sardina et al., 2012) and a turbulent concentration-vertical acceleration interaction terms. Thus, the revision to the widely used Equation 4 depends on the overall significance of $\Phi(z)$ at any z. The magnitude of $\Phi(z)$ varies with the local Stokes number $St(z) = \tau_0/\tau_k(z)$ where $\tau_k(z) = [\nu/\epsilon(z)]^{1/2}$ is the Kolmogorov time scale formed by the local turbulent kinetic energy dissipation rate $\epsilon(z)$ and ν as reviewed elsewhere (Bragg et al., 2021). An associated length scale to τ_K is $\eta = (v^3/\epsilon)^{1/4}$, which is the Kolmogorov micro-scale representing eddy sizes impacted by viscous effects at z. Upon defining the Kolmogorov velocity as $v_k = \eta/\tau_k$, the Kolmogorov micro-scale Reynolds number $Re_k = v_k \eta/\nu = 1$, meaning that both turbulence and viscous effects are equally important at scales commensurate to η (Tennekes & Lumley, 1972). In the limit $St \to 0$, the particle vertical velocity is w - w and $\Phi(z)$ can be ignored relative to the turbulent flux at z, an assumption routinely invoked in operational models for SSC. To allow for a "bulk" Stokes number St_b to be formulated thereby facilitating comparisons across experiments, $\tau_{K,b} = (v/\epsilon_b)^{1/2}$ is proposed where ϵ_h is the over-all bulk dissipation rate in clear water. Thermodynamic considerations alone allow for an estimate of ϵ_b from bulk variables. The work per unit mass per unit time necessary to move clear water at U_b is $(gS_o)U_b$. For steady-state conditions (i.e., turbulent kinetic energy is stationary), this mechanical work produces turbulence that is then dissipated by the action of viscosity leading to an increase in the internal energy of the fluid. Hence,

$$\epsilon_b = (gS_o)U_b; \quad \tau_{K,b} = \sqrt{\frac{v}{\epsilon_b}}; \quad \text{and} \quad St_b = \left(\frac{w_s}{g}\right)\tau_{K,b}^{-1}.$$
 (6)

It is assumed that Φ is small and can be ignored when $St_b \ll 1$ (although, more precisely, Φ can only be ignored when $\max[St_b, St] \ll 1$). Another estimate of bulk Stokes number is $St_+ = \tau_p(u_*/H)$ (Greimann et al., 1999; Greimann & Holly, 2001), where (H/u_*) is presumed to represent a large eddy turnover time given its dependency on H. Noting that $gS_o = u_*^2/H$, the two bulk Stokes numbers can be related using $St_b = St_+(Re_b)^{1/2}$. A critique for using St_+ as a bulk Stokes number measure to discard Φ everywhere has already been discussed (Greimann et al., 1999; Richter & Chamecki, 2018).

With regards to the terminal sediment velocity, a simplified expression for w_s that recovers many prior formulae (W. Huai et al., 2020; Tan et al., 2018) is used here and is given by (Cheng, 1997)

$$w_s = \frac{v}{d_s} \left[\sqrt{25 + 1.2d_s^2 \left(\frac{\rho_s - \rho}{\rho} \frac{g}{v^2} \right)^{2/3}} - 5 \right]^{3/2}, \tag{7}$$

where ρ_s is the sediment grain density with $\rho_s/\rho > 1$, and d_s is the sediment grain diameter. This w_s is smaller than the Stokes settling velocity (w_{sr})

LI ET AL. 3 of 19

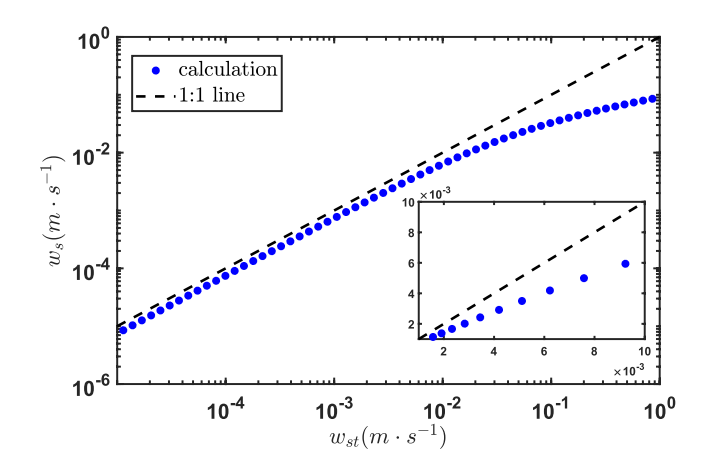


Figure 1. Comparison between the empirical sediment settling velocity w_s used here and the Stokes settling velocity w_{st} for different sediment to fluid density ratios. The one-to-one line is presented for reference. The comparison between w_s and w_{st} for the data sets explored here is also featured as inset.

$$w_{st} = \frac{1}{18} \frac{g}{v} \left(\frac{\rho_s - \rho}{\rho} \right) d_s^2, \tag{8}$$

except when the sediment particle Reynolds number $Re_{sp} = w_s d_s / \nu \ll 1$. The difference between the two settling velocity formulations can be understood when the balance between the gravitational force and a quadratic drag force acting on a spherical grain is considered. This balance is given by

$$(\rho_s - \rho) g \frac{4}{3} \pi \left(\frac{d_s}{2}\right)^3 = \frac{1}{2} \rho C_{d,p} \left[\pi \left(\frac{d_s}{2}\right)^2 \right] w_s^2, \tag{9}$$

where $C_{d,p}$ is the drag coefficient of the sediment particle. The Stoke's formulation is recovered when $C_{d,p} = 24Re_{sp}^{-1}$ for creeping flow whereas Equation 7 assumes a non-linear relation between $C_{d,p}$ and Re_{sp}^{-1} derived from published experiments for sediments across a wide range of Re_{sp} and d_s . The functional

form of this non-linear relation is given by $C_{d,p} = \left[(A_p/Re_{sp})^{1/n'} + (B_p)^{1/n'} \right]^{n'}$, where $A_p = 32$ (instead of 24 for smooth spheres), $B_p = 1$, and n' = 3/2. As Re_{sp} becomes large, form drag instead of viscous drag dominates and $C_{d,p} \rightarrow 1$ (a constant) whereas the Stokes formulation extrapolation predicts a $C_{d,p} \rightarrow 0$ (or the viscous sublayer thickness becomes infinitely thin on a

perfectly smooth sphere). The comparison between the two settling velocities is shown in Figure 1 for reference. Since w_{st} only applies to creeping flow past a sphere, Equation 7 is used as it covers a wider range of $w_{st}d/\nu$.

The mode of sediment transport is operationally related to w_s and some measure of the strength of turbulence based on bulk flow properties. One such measure is the Rouse number R or "unit" Rouse number R_* given by

$$R^* = \frac{1}{\kappa} \frac{w_s}{u_*}; \quad R = \frac{1}{\beta} R^*; \tag{10}$$

where $\kappa = 0.41$ is the von Kármán constant and $\beta = Sc^{-1}$ is an inverse turbulent Schmidt number (Sc). The Rouse number is routinely used for classifying sediment load: R > 2.5 for bedload, 0.8 < R < 2.5 for SS (the focus here), and R < 0.8 for washload. To solve for \overline{C} , models linking $\overline{w'C'}$ to \overline{C} as well as estimates for Sc (and Φ , though this is ignored here) are required in Equation 4, and those models are to be briefly covered.

2.2. Conventional Formulations and Revisions

Conventional approaches (O'Brien, 1933; Rouse, 1939) for modeling SSC begin by ignoring $\Phi(z)$ and employing a gradient-diffusion approximation (or some non-Fickian revision to it) given as

$$\overline{w'C'} = -D_s \frac{d\overline{C}}{dz},\tag{11}$$

where D_s is the sediment turbulent diffusivity. To estimate $D_s(z)$, existing theories approximate $D_s(z)$ by ν_t/Sc or $\beta\nu_t$, where ν_t is the turbulent or eddy viscosity ($\nu/\nu \gg 1$). When the mixing length hypothesis is further invoked to model ν_t as a product of a characteristic length and velocity, it yields

$$v_t = l_o \left(l_o \left| \frac{d\overline{u}}{dz} \right| \right), \tag{12}$$

where l_o is a generic mixing length to be externally supplied that can vary with z (can be piecewisely determined in different flow and channel conditions as in Li & Katul, 2020). Dimensional analysis and similarity theory represent

$$\frac{d\overline{u}}{dz} = \frac{\sqrt{-\overline{u'w'}(z)}}{l_o(z)},\tag{13}$$

LIET AL. 4 of 19



where u' is the longitudinal velocity fluctuation, and $\overline{u'w'}$ is the momentum turbulent flux at height z that can be estimated from the mean momentum balance using (Dey, 2014)

$$\frac{-\overline{u'w'}(z)}{u_*^2} = (1 - z_n),$$
 (14)

where $z_n = z/H$ is the normalized water depth. With this estimate of $\overline{u'w'}(z)$, it follows directly that

$$\frac{d\overline{u}}{dz} = \frac{u_*}{l_o} (1 - z_n)^{1/2}; v_t = u_* l_o (1 - z_n)^{1/2}; D_s = \beta u_* l_o (1 - z_n)^{1/2}.$$
(15)

These expressions ensure that as $z_n \to 1$, $d\bar{u}/dz \to 0$, $v_t \to 0$, and $D_s \to 0$. For $z_n \ll 1$ but $z^+ > 50$ (i.e., above the buffer layer) where $z^+ = zu_*/\nu$ is a normalized distance in wall units (Pope, 2000) that can also be interpreted as a local Reynolds number (Re_s) , l_o is constrained by the channel bottom so that $l_o = \kappa z$. In this case, $d\bar{u}/dz \approx u_*/(\kappa z)$ and $\bar{u}(z)$ varies logarithmically with z, $\nu_t = \kappa zu_*$, and $D_s = \beta \kappa zu_*$ (i.e., linear in z). As $z_n \to 1$, the largest eddies are restricted by H so that $l_o \propto H$ instead of z. Combining these two arguments using $l_o = \kappa z(1 - z_n)^{1/2}$ yields the quadratic diffusivity profile reported in a number of stream flow studies (Fischer et al., 2013) and direct numerical simulations (DNS) of stratified atmospheric flows on inclined planes (Giometto et al., 2017). Assuming $\beta = Sc^{-1} = 1$, the SSC profiles associated with the linear and quadratic $D_s(z)$ are

$$\frac{\overline{C}(z_n)}{\overline{C_b}} = \left(\frac{z_n}{z_{n,b}}\right)^{-R^*}, \text{ linear diffusivity, Prandtl's formula}$$

$$\frac{\overline{C}(z_n)}{\overline{C_b}} = \left(\frac{z_n}{1 - z_n} \frac{1 - z_{n,b}}{z_{n,b}}\right)^{-R^*}, \text{ quadratic diffusivity, Rouse's formula,}$$
(16)

where $\overline{C_b}$ is a reference concentration at height $z_{n,b} = z_b/H$ and $R_* = R$ when setting $\beta = 1$. The R_* in Equation 16 is commonly replaced by a fitted R (or β is no longer unity) as discussed elsewhere (Dey, 2014; Muste et al., 2005). The analysis using fitted R is termed here as 'fitted' Rouse's formula. Other models for l_o have been introduced but only two are singled out here for illustrating differences in approaches to adjusting conventional formulations (usually for κz): (a) $l_o = \kappa z V_n(z_n)$, where $V_n = 1 - \exp(-z^+/26)$ (labeled as the van Driest damping function); (b) $l_o = \kappa z (1 - z_n)^{m_1}$, where

$$m_1 = \frac{1}{2} \left[1 + a_e \left(\frac{\overline{C}}{C_R} \right) \right],\tag{17}$$

 C_R is some reference concentration and a_e is an empirical coefficient (Castro-Orgaz et al., 2012; Mazumder & Ghoshal, 2006; Umeyaina, 1992). In the second case, the mixing length is assumed to vary with SSC and recovers $l_o = \kappa z (1-z_n)^{1/2}$ only for clear water. However, in the presence of sediments, m_1 varies with z_n (and R). In the first case, deviations from a linear mixing length is made to dependent on z^+ (instead of H), which is appropriate in the viscous and buffer regions of smooth boundary layers. Another revision to Equation 11 is to recast turbulent transport in fractional derivatives to emphasize its non-Fickian aspect (Nie et al., 2017). In this approach, the fractional order becomes a parameter that must be determined from experiments depending on how SS trajectories deviate from Brownian trajectories (Sun et al., 2020). In practice, the order of the fractional derivative is set as a 'free' parameter and must implicitly include the Sc effect. This approach is not pursued further here.

2.3. Turbulent Stress and SS Flux Budgets

Simplified turbulent stress and SS flux budgets are now considered. For a stationary and planar homogeneous flow in the absence of subsidence ($\overline{w} = 0$), these budgets reduce to

$$\frac{\partial \overline{w'u'}}{\partial t} = 0 = -\overline{w'w'}\frac{\partial \overline{u}}{\partial z} - \frac{\partial \overline{w'w'u'}}{\partial z} + \overline{p'}\frac{\partial u'}{\partial z} - \epsilon_{wu},$$

$$\frac{\partial \overline{w'C'}}{\partial t} = 0 = -\overline{w'w'}\frac{\partial C}{\partial z} - \frac{\partial \overline{w'w'C'}}{\partial z} + \overline{p'}\frac{\partial C'}{\partial z} - \epsilon_{wc} - w_s \left(\overline{w'}\frac{\partial C'}{\partial z}\right),$$
(18)

LI ET AL. 5 of 19



where p' is the turbulent pressure, ϵ_{wu} and ϵ_{wc} are molecular destruction terms assumed to be small when compared to the pressure-decorrelation terms at high Reynolds numbers (Katul et al., 2013). The turbulence-particle interaction term requires closure. Here, a new closure approach is proposed that commences with a local decomposition given by

$$w_{s}\overline{\left(w'\frac{\partial C'}{\partial z}\right)} = w_{s}\left[\left(\frac{\partial \overline{w'C'}}{\partial z}\right) - \left(\overline{C'\frac{\partial w'}{\partial z}}\right)\right]. \tag{19}$$

When assuming $\Phi(z) = 0$ (i.e., no particle inertia), $\overline{w'C'} = w_s \overline{C}$ thereby allowing one of the two terms in the difference shown in Equation 19 to be linked to variables that are explicitly modeled. The other term (i.e., $\overline{C'\partial w'/\partial z}$) still necessitates a closure. A heuristic model that maintains maximum simplicity is now proposed by setting

$$\overline{C'\frac{\partial w'}{\partial z}} = b_1 \frac{\partial \overline{w'C'}}{\partial z},\tag{20}$$

where b_1 is a positive or a negative constant. Upon setting $\overline{w'C'} = w_s \overline{C}$, this heuristic closure model recovers a similar closure scheme used for particles (Huang et al., 2014) and is given by

$$w_{s}\overline{\left(w'\frac{\partial C'}{\partial z}\right)} = w_{s}\left[\left(\frac{\partial w_{s}\overline{C}}{\partial z}\right) - b_{1}\left(\frac{\partial w_{s}\overline{C}}{\partial z}\right)\right] = \alpha'w_{s}^{2}\frac{\partial\overline{C}}{\partial z},\tag{21}$$

where $\alpha' = 1 - b_1$ is assumed to be a constant. When $|b_1| \ll 1$, then $\alpha' = 1$ and

$$w_s \overline{\left(w' \frac{\partial C'}{\partial z}\right)} = w_s^2 \frac{\partial \overline{C}}{\partial z}.$$
 (22)

Whether b_1 or α' are strictly closure constants independent of sediment and/or flow conditions cannot be a priori ascertained. To do so requires another scaling analysis based on different assumptions and approximations. In this proposed scaling analysis, C' is assumed to vary with a turbulent quantity such as σ_c , and w' to vary with σ_w . Hence,

$$\overline{\left(C'\frac{\partial w'}{\partial z}\right)} = A_F \left[\sigma_c(z)\right] \frac{\partial \sigma_w}{\partial z} = A_F \left[\overline{w'C} \atop u_* F_1(z_n)\right] \frac{\partial \sigma_w}{\partial z},$$
(23)

where A_F is a flux-variance (Albertson et al., 1995) similarity constant that can be positive or negative depending on the sign of the correlation coefficient between C' and $\partial w'/\partial z$, and $F_1(z_n)$ is an unknown dimensionless function describing the sediment concentration variance with z_n above and beyond the $\overline{w'C'}$ variations with z_n . Since the goal is to determine the minimum governing variables impacting b_1 or α' while assuming b_1 is independent of z_n , Equations 23 and 20 can be equated to yield

$$A_{F}\left[\frac{\overline{w'C'}(z_{n})}{u_{*}}F_{1}(z_{n})\right]\frac{\partial\sigma_{w}}{\partial z} = b_{1}\frac{\partial\overline{w'C'}(z_{n})}{\partial z}.$$
(24)

Re-arranging to infer b_1 results in

$$b_{1} = A_{F} \left[\overline{w'C'} \left(\frac{\partial \overline{w'C'}}{\partial z} \right)^{-1} \right] \left[\frac{1}{u_{*}} F_{1} \left(z_{n} \right) \frac{\partial \sigma_{w}}{\partial z} \right]. \tag{25}$$

With the assumption that b_1 is not dependent on z_n , additional order of magnitude arguments must now be invoked to assess the sediment/flow variables that impact its magnitude: (a) $\partial \sigma_w/\partial z \sim -u_*/H$ (likely valid except near the channel bottom), (b) F_1 is roughly a constant, (c) $\partial \overline{w'C'}/\partial z = w_s \partial \overline{C}/\partial z$, and (d) $\overline{w'C'}/\left(\partial \overline{C}/\partial z\right) \sim -D_{s,avg}$ where $D_{s,avg} = (1/H) \int_0^H D_s(z) dz \sim u_*H$. Inserting these order of magnitude arguments into Equation 25 result in

$$b_1 \sim \operatorname{sgn}(A_f) \frac{u_* H}{w_s} \left[\frac{1}{u_*} \frac{u_*}{H} \right] \sim \operatorname{sgn}(A_f) \frac{u_*}{w_s}, \tag{26}$$

LI ET AL. 6 of 19



where sgn indicates the sign of the variable. Equation 19 is used to suggest a pragmatic closure in Equation 21 that applies to only one of two terms, and this one term itself is only one term in the overall flux budget. Given the interplay between these multiple terms, the overall model results for \overline{C} may be robust to uncertainties in this closure vis-a-vis externally imposing Sc or β^{-1} directly on the eddy diffusivity as common in prior models (e.g., Rouse-O'Brien).

Upon ignoring the flux transport terms (triple moments), and closing the pressure decorrelation terms using a linear Rotta scheme that accounts for the isotropization of the production simplify Equation 19 to

$$-(1-C_I)\sigma_w^2 \frac{\partial \overline{u}}{\partial z} - A_R \frac{\overline{w'u'}}{\tau} = 0, \quad \left[-(1-C_I) - \alpha' \frac{w_s^2}{\sigma_w^2} \right] \sigma_w^2 \frac{\partial \overline{C}}{\partial z} - A_R \frac{\overline{w'C'}}{\tau} = 0, \tag{27}$$

where τ is a turbulent relaxation time scale, $C_I = 3/5$ is the isotropization of the production constant determined from rapid distortion theory (Pope, 2000), and $A_R = 1.8$ (Katul et al., 2013; Katul & Manes, 2014) is the Rotta constant assumed to be the same for momentum and SS. It directly follows from these simplified budgets that a model of maximum simplicity for Sc may be derived as

$$Sc^{-1}(z_n) = \frac{D_s}{v_t} = 1 + \alpha \left(\frac{w_s}{\sigma_w}\right)^2, \tag{28}$$

where $\alpha = \alpha'/(1 - C_I)$, though α' or b_1 can vary themselves with u_*/w_s as noted earlier. It is necessary to point out that when $\alpha \ge 0$, Equation 28 is opposite to what is predicted by the so-called 'crossing-trajectories' effect for heavy particles settling in a turbulent flow. The crossing trajectories arise when particle trajectories cross trajectories of fluid elements under the influence of gravity. This effect invariably forces particles to move from a region of highly correlated flow to another less correlated region (Wells & Stock, 1983). In this manner, particles lose velocity correlation more rapidly than the corresponding fluid points and thus must disperse less. Thus, the crossing trajectories effect requires Sc > 1 (Csanady, 1963; Duman et al., 2016).

To summarize, Equation 27 demonstrates how the turbulent fluxes of momentum and SSC can be modeled as a function of the mean gradients as

$$\overline{w'u'} = -\frac{(1 - C_I)}{A_R} \tau \sigma_w^2 \frac{\partial \overline{u}}{\partial z}; \quad \overline{w'C'} = -\frac{(1 - C_I)}{A_R} \left[1 + \alpha \frac{w_s^2}{\sigma_w^2} \right] \tau \sigma_w^2 \frac{\partial \overline{C}}{\partial z}, \tag{29}$$

where the eddy diffusivity for momentum varies with $\tau \sigma_w^2$ requiring specification with z_n . The same analysis is now revisited in spectral space thereby allowing models for τ , σ_w^2 , and Sc to be formulated based on the canonical shape of the spectrum of vertical velocity in turbulent boundary layers and a local balance between turbulent kinetic energy generation and destruction at any z_m .

2.4. The Co-Spectral Budget Model

The models so far make no explicit contact with the phenomenon they perpetrate to represent: turbulent eddies and their energy distribution. The proposed approach here uses a CSB to establish such a link. The CSB is derived from an approximated Navier-Stokes equation in a spectral form that links turbulent eddies of different sizes to $\overline{w'C'}$. The CSB derivation commences by noting that $\overline{w'C'}$ and $\overline{u'w'}$ both satisfy the normalizing properties,

$$-\overline{w'C'} = \int_0^\infty \phi_{wc}(k)dk, \quad -\overline{u'w'} = \int_0^\infty \phi_{wu}(k)dk, \tag{30}$$

where $\phi_{wc}(k)$ and $\phi_{wu}(k)$ are the co-spectral density functions of the turbulent vertical velocity-turbulent sediment concentration and turbulent vertical-longitudinal velocities, respectively, and k is the wavenumber or inverse eddy size. The co-spectral budgets associated with Equation 19 have been derived elsewhere and simplify to (Bos et al., 2004; Cava & Katul, 2012; Katul et al., 2013; Katul & Manes, 2014; Li & Katul, 2021),

$$\frac{\partial}{\partial t}\phi_{wu}(k) = 0 = P_{wu}(k) + T_{wu}(k) + \pi_{wu}(k) - 2\nu k^2 \phi_{wu}(k), \tag{31}$$

$$\frac{\partial}{\partial t}\phi_{wc}(k) = 0 = P_{wc}(k) + T_{wc}(k) + \pi_{wc}(k) - \nu \left(1 + Sc_m^{-1}\right) k^2 \phi_{wc}(k), \tag{32}$$

LI ET AL. 7 of 19



where $P_{wu}(k) = \left(d\overline{u}/dz\right)E_{ww}(k)$ and $P_{wc}(k) = \left(d\overline{C}/dz\right)E_{ww}(k)$ are the stress and flux production terms at k, $E_{ww}(k)$ is the vertical velocity spectrum satisfying the normalizing relation $\sigma_w^2 = \int_0^\infty E_{ww}(k)dk$, $T_{wu}(k)$ and $T_{wc}(k)$ are turbulent transfer terms, $\pi_{wu}(k)$ and $\pi_{wc}(k)$ are pressure-velocity and pressure-scalar decorrelation terms, and Sc_m is the molecular Schmidt number (not related to Sc). Invoking a spectral-based Rotta model that includes the isotropization of the production as before, the pressure-scalar co-variance in k-space can be modeled as

$$\pi_{wu}(k) = -A_R \frac{1}{t_{ww}(k)} \phi_{wu}(k) - C_I P_{wu}(k), \quad \pi_{wc}(k) = -A_R \frac{1}{t_r(k)} \phi_{wc}(k) - C_I P_{wc}(k), \tag{33}$$

where $A_R \approx 1.8$ and $C_I = 3/5$ are as before, $t_{ww}(k)$ and $t_r(k)$ are the decorrelation time-scale of the turbulent stress and particle concentration. Because of inertia, the $t_r(k)$ differs from $t_{ww}(k)$ in a number of ways as already fore-shadowed from Equation 28. A model of maximum simplicity is to assume that these two wavenumber dependent time scales are related using a wavenumber-dependent Sc(k) given by,

$$t_r(k) = t_{ww}(k)Sc^{-1}(k), \text{ with } Sc^{-1}(k) = 1 + \alpha(w_s k t_{wc})^2,$$
 (34)

where $t_{wc} = \min(t_{ww}, f_o \ t_{K,b})$ with f_o being a constant (a plausibility argument to such $t_{wc}(k)$ representation is discussed later), and Sc(k) is modeled in analogy to Equation 28 albeit in spectral form. That is, Sc is based on a local scale-wise characteristic turbulent velocity estimated by $(kt_{wc})^{-1}$ using a one-way coupling approach (Elghobashi, 1994). The $t_{ww}(k) \propto e^{-1/3}k^{-2/3}$ is interpreted as a characteristic time scale derived from dimensional analysis assuming e is the conserved quantity across the energy cascade of $E_{ww}(k)$, and e is the turbulent kinetic energy dissipation rate. One plausible choice for the proportionality constant is $C_o^{-1/2}$ so as to recover a Kolmogorov time scale in the inertial subrange, where $C_o = 0.65$ is the Kolmogorov constant for the vertical velocity component.

For scalewise integration, it is also necessary to maintain a bounded $t_r(k)$ as $k \to 0$ for any z_n . We set $t_r(k) = t_r(k_c)$ when $k < k_c$, where k_c is the smallest inverse length scale where $E_{ww}(k)$ increases with increasing k. The viscous-destruction terms are negligible when compared to the Rotta terms for $k\eta \ll 1$. Since $T_{wu}(k)$ and $T_{wc}(k)$ do not contribute to the net production or destruction of $\phi_{wu}(k)$ and $\phi_{wc}(k)$ but only redistribute them across scales (i.e., $\int_0^\infty T_{wu}(k)dk = 0$, and $\int_0^\infty T_{wc}(k)dk = 0$), they are ignored for simplicity (Bonetti et al., 2017). Adopting these simplifications,

$$\phi_{uw}(k) = \left(\frac{1 - C_I}{A_R}\right) \frac{d\overline{u}}{dz} \left[E_{ww}(k) t_{ww}(k) \right], \quad \phi_{wc}(k) = \left(\frac{1 - C_I}{A_R}\right) \frac{d\overline{C}}{dz} \left[E_{ww}(k) t_r(k) \right]. \tag{35}$$

To integrate these equations across k and derive turbulent shear stress and sediment flux at any height z_n , an expression for $E_{ww}(k)$ is required. A model for $E_{ww}(k)$ that captures known spectral features at an arbitrary z_n is shown in Figure 2.

The $E_{ww}(k)$ is now piece-wise approximated as

$$E_{ww}(k) = \begin{cases} E_{kol}(k_o) k_c^{-2} k^2, & \text{if } 0 \le k \le k_c \\ E_{kol}(k_o), & \text{if } k_c \le k \le k_o, \\ E_{kol}(k), & \text{if } k_o \le k \le k_e \end{cases}$$
(36)

where $k_c = H^{-1}$, $k_o = (\kappa z)^{-1}$ and $k_e = \eta^{-1}$ are three characteristic wavenumbers that mark the key transitions in $E_{ww}(k)$ between H and the characteristic eddy scales bounding the inertial subrange (Ayet & Katul 2020; Bonetti et al., 2017; Katul et al., 2013; S. Li & Katul, 2019), and $E_{kol}(k) = C_o \varepsilon(z)^{2/3} k^{-5/3}$ is the Kolmogorov spectrum. In the case of $E_{kol}(k)$, the transfer of energy across scales shapes the energy cascade and is necessary for obtaining the $k^{-5/3}$ scaling. The transfer of stress across scales, as given by $T_{wu}(k)$, was ignored in the CSB model here. The inclusion of the transfer term in the energy cascade (indirectly specified by $E_{ww}(k)$) but not in the CSB may appear paradoxical. This is not so as the role and significance of the transfer terms are quite different when analyzing scale-wise energy and stress budgets (Bos et al., 2004). In the inertial subrange where $E_{kol}(k) \sim k^{-5/3}$, a $\phi_{uw}(k) \sim k^{-7/3}$ has also been reported and confirmed in numerous boundary layer experiments and simulations of wall-bounded flows (Pope, 2000). A balance between production and dissipation terms in the CSB model leads

LI ET AL. 8 of 19

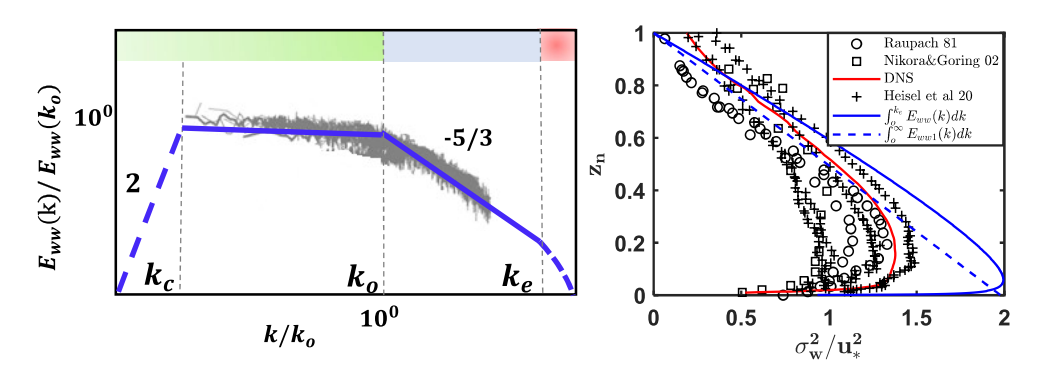


Figure 2. Left: A typical $E_{ww}(k)$ at z_n from the channel bottom. The very low wavenumber range are assumed to follow the Saffman spectrum ($E_{ww}(k) \propto k^2$) until $k_c = 1/H$. The Saffman spectrum is then connected using a flat transition (i.e., wall effects introduce energy splashing) to the inertial subrange at $k_o \propto 1/z$ where $E_{ww}(k) \propto k^{-5/3}$. The black curves are extracted from measurements (Nikora & Goring, 2002) with different flow conditions using acoustic Doppler velocity and do not resolve the viscous dissipation range in the vicinity of $k_e = 1/\eta$ or the presumed Saffman spectrum. Right: The σ_w^2/u_*^2 profile modeled from scale-wise integration of $E_{ww}(k)$ and its simplified form ($E_{ww}(k)$), that is, ignoring the Saffman contribution and extending the inertial subrange indefinitely to fine scales). The measured σ_w^2/u_*^2 profiles are from experiments described elsewhere (Heisel et al., 2020; Nikora & Goring, 2002; Raupach, 1981). They include field experiments and wind-tunnel experiments over a wide range of roughness types and Reynolds number conditions. The direct numerical simulations (DNS) for a smooth channel (red) are also included for comparisons (Heisel et al., 2020).

to a $\phi_{uw}(k) \sim \left(d\overline{u}/dz\right) E_{ww}(k) t_{ww}(k)$, which recovers the $\left[\left(d\overline{u}/dz\right) \epsilon^{1/3}\right] k^{-7/3}$ scaling in the inertial subrange. Inclusion of $T_{wu}(k)$ necessarily leads to $\phi_{uw}(k)$ that must deviate from a $k^{-7/3}$ scaling in the inertial subrange as discussed elsewhere (Li et al., 2015). Moreover, the constants emerging from a production balancing dissipation in the scale-wise CSB model for the inertial subrange, $\left[\left(1-C_I\right)/A_R\right]C_o^{1/2}=0.18$, does recover the accepted co-spectral similarity constant whose numerical value was determined at 0.15–0.16 from wind tunnel studies, atmospheric surface layer studies, and DNS (Katul et al., 2013). For these reasons (i.e., $T_{wu}(k)$ ignored within the inertial subrange) and because $\int_0^\infty T_{wu}(k) dk = 0$, $T_{wu}(k)$ is ignored at all k. This assumption is also compatible with ignoring the triple moments in Equation 19.

The only remaining term needed to describe the magnitude of $E_{ww}(k)$ at all k is $\epsilon(z)$. A model of maximum simplicity is to relate $\epsilon(z)$ to the mechanical production $P_{TKE}(z)$ of the turbulent kinetic energy budget using (Pope, 2000)

$$\varepsilon(z) = \frac{P_{TKE}(z)}{\phi(z_n)} = \phi^{-1}(z_n) \left(-\overline{u'w'} \frac{d\overline{u}}{dz} \right) = \phi^{-1}(z_n) u_*^2 \left(1 - \frac{z}{H} \right) \frac{d\overline{u}}{dz}, \tag{37}$$

where $\phi(z_n)$ is a modification function to account for the imbalance between the local mechanical production and local dissipation terms in the turbulent kinetic energy budget. For stationary and planar-homogeneous flow conditions without any mean vertical advection and in the absence of any transport terms, $\epsilon(z) \approx P_{TKE}(z)$ and $\phi(z_n) \approx 1$. While this estimate may be acceptable in the log-region describing $\overline{u}(z)$, deviations near the channel bottom $(\phi(z_n) > 1)$ and near the water surface $(\phi(z_n) < 1)$ are expected. Hence, $\phi(z_n)$ must be viewed as a depth-dependent function (Kim et al., 1987; Pope, 2000) though its variation from unity is not considered here to maintain maximum simplicity. A plausibility argument for ignoring its variation from unity is that $\overline{w'C'} \propto [\phi(z_n)]^{-1/3}$ (shown later), which makes the SSC calculations less sensitive to $\phi(z_n)$ deviations from unity. This point is considered later in the context of modeling $\sigma_w^2(z_n)$ based on the assumed $E_{ww}(k)$ shape.

Returning to the choice of $t_{wc} = \min(t_{ww}, f_o t_{K,b})$ and the choice f_o , as $z_n \to 1$, $\overline{w'u'} \to 0$, $P_{TKE}(z_n) \to 0$, and thus $\epsilon \to 0$ (i.e., no turbulence) near the free water surface. With $\epsilon \to 0$, $t_{ww}(k) \to \infty$ (along with $\tau_k \to \infty$ and $\eta_k \to \infty$). That $t_{ww}(k) \to \infty$ is not problematic for the closure scheme of $\pi_{wu}(k)$ and $\pi_{wc}(k)$ as those terms are expected to decay near the free water surface and this decay remains compatible with $t_{ww}(k) \to \infty$. The problem of $\epsilon \to 0$ arises in maintaining a finite $Sc^{-1}(k)$ dominated by turbulent processes thereby necessitating a finite ϵ in the calculation of $Sc^{-1}(k)$ that cannot be readily inferred from $P_{TKE}(z_n)$. To ensure that the particle interaction time scale t_{wc} remains bounded in $Sc^{-1}(k)$, an adhoc minimal value of ϵ , set to be 0.1% ϵ_b , is proposed. This choice of minimal ϵ_b prevents $\epsilon \to 0$ as $z_n \to 1$ in the Sc(k) formulation only. This minimal threshold set to ensure a finite ϵ in Sc(k)

LI ET AL. 9 of 19



(mainly near the free water surface) leads to $f_o = \sqrt{1000} \approx 31$. Changing the threshold 0.1% ϵ_b to smaller values simply reduces the thickness of the region directly impacted by the free water surface in the vicinity of $z_n = 1$ but the solution in all other regions is not directly impacted by this choice.

3. Results and Discussion

3.1. Co-Spectral Budget Model

By scale-wise integrating $\phi_{uv}(k)$ and using $u_*^2(1-z_n) = \int_0^{k_e} \phi_{uw}(k) dk$, the velocity gradient $d\overline{u}/dz$ at z is obtained as

$$\frac{d\overline{u}}{dz} = A_{\pi}^{-3/4} \phi^{1/4}(z_n) \left(1 - \frac{z}{H}\right)^{1/2} \left[\frac{15}{4} - \frac{8}{3} \left(\frac{k_c}{k_o}\right)^{1/3} - \frac{3}{4} \left(\frac{k_o}{k_e}\right)^{4/3} \right]^{-3/4} (k_o u_*), \tag{38}$$

where $A_{\pi} = (1 - C_I) \sqrt{C_o} / A_R \approx 0.18$, and the vertical velocity variance can be derived by scale-wise integrating $E_{---}(k)$ as,

$$\frac{\sigma_w^2}{u_*^2} = \frac{5}{2} C_o A_\pi^{-1/2} \phi^{-1/2}(z_n) \left[1 - \frac{4}{15} \frac{k_c}{k_o} - \frac{3}{5} \left(\frac{k_e}{k_o} \right)^{-2/3} \right] \left[\frac{15}{4} - \frac{8}{3} \left(\frac{k_c}{k_o} \right)^{1/3} - \frac{3}{4} \left(\frac{k_e}{k_o} \right)^{-4/3} \right]^{-1/2} (1 - z_n). \tag{39}$$

Likewise, the SSC turbulent flux is solved as

$$-\overline{w'C'} = A_{\pi}\phi^{-1/3}(z_n)\Omega(z_n)u_*^{2/3} \left[\left(1 - \frac{z}{H}\right)\frac{d\overline{u}}{dz} \right]^{1/3} \frac{d\overline{C}}{dz} = -w_s\overline{C}, \tag{40}$$

with $\Omega(z_n)$ given by

$$\Omega(z_n) = \int_0^{k_c} Sc^{-1}(k_c) k_c^{-8/3} k_o^{-5/3} k^2 dk + \int_{k_c}^{k_o} k_o^{-5/3} Sc^{-1}(k) k^{-2/3} dk + \int_{k_c}^{k_e} Sc^{-1}(k) k^{-7/3} dk.$$
 (41)

The turbulent Schmidt number at any z_n can be determined from $\nu_t(z_n)$ in Equation 38 and from $D_s(z_n)$ in Equation 40 using

$$Sc(z_n) = \frac{v_t}{D_s} = \Omega^{-1}(z_n) \left[\frac{15}{4} - \frac{8}{3} \left(\frac{k_c}{k_o} \right)^{1/3} - \frac{3}{4} \left(\frac{k_o}{k_e} \right)^{4/3} \right] k_o^{-4/3}. \tag{42}$$

Because the determination of $k_e = 1/\eta$ (where $\eta = \left(v^3/\epsilon\right)^{1/4}$) requires an estimate of $\epsilon(z_n) = P_{uw}(z_n)$ and thus an estimate of $d\overline{u}/dz$, an iterative scheme is needed to determine $d\overline{u}/dz$ and k_e at every z_n from Equation 38. Once determined, the $E_{ww}(k)$, $Sc(z_n)$, $\overline{w'C'}$ and the subsequent SSC profile can be computed at each z_n by solving Equations 39, 40 and 42 for σ_w^2 , $\overline{w'C'}$ and Sc. Since there is no analytical solution to this system, a numerical integration using a third-order Adams–Bashforth method is employed.

Before proceeding to the analysis of SSC, an assessment of the assumed shape of $E_{ww}(k)$, its transition wavenumbers, as well as the consequence of the assumption of $\phi(z_n) \approx 1$ is conducted in Figure 2. The predicted σ_w^2/u_*^2 from Equation 39, and its simplified version using $E_{ww1}(k)$ without the Saffman spectrum and assuming $k_e/k_c \rightarrow \infty$ are compared against two sets of experiments: (a) wind tunnel experiments conducted over a wide range of surface roughness types (Raupach, 1981) and (b) field experiments (Nikora & Goring, 2002) of the sediment flow in the Balmoral Irrigation Canal (New Zealand). The wind-tunnel experiments used a hot-wire probe whereas the field experiments used ADV measurements that do not resolve the viscous dissipation regime. As expected, the predicted σ_w^2/u_*^2 here exceeds the measurements because the spectral shapes assumed in $E_{ww}(k)$ account for a much broader range of eddy sizes than the experiments interrogate. Specifically, the Saffman and dissipation ranges are not resolved by the flume experiments whereas the wind tunnel experiments resolve a limited dissipation range but are not conducted over a sufficiently long enough sampling period to cover the Saffman spectrum. The inclusion of the Saffman spectrum here ensures that σ_w^2 remains finite near the water surface whereas the turbulent stress is not. The simplified model for $E_{ww}(k)$, when integrated at any z_n , recovers key features of the $(\sigma_w/u_*)^2$ profile: a rapid increase with z_n near the surface, a peak at $(\sigma_w/u_*)^2 = 1.9$, and a quasi-linear decline as

LI ET AL. 10 of 19



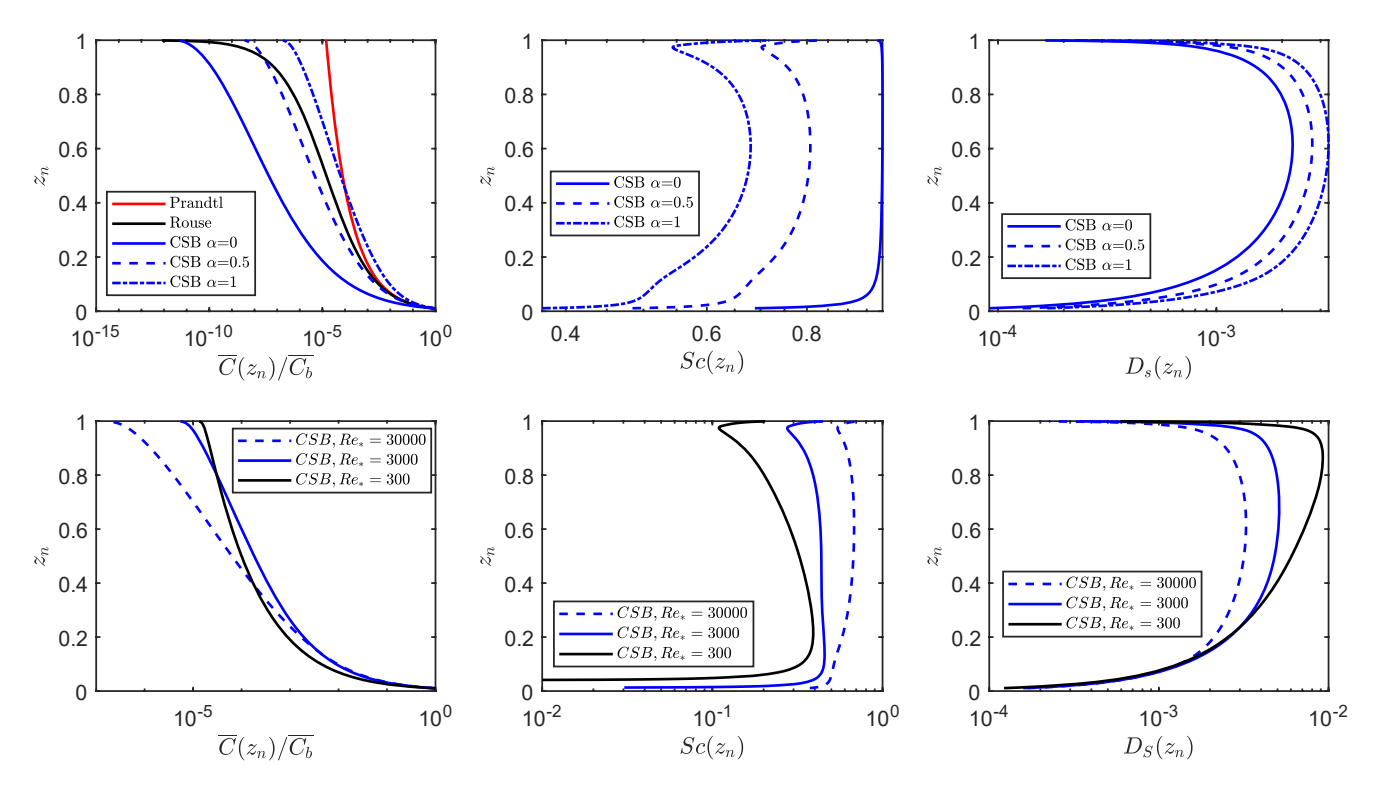


Figure 3. The predicted suspended sediment concentration (SSC), Sc, and D_s profiles based on the co-spectral budget (CSB) model of Section 3.1 when setting $d_s = 1 \text{ mm}$, $\rho_s = 1.2 \text{ g cm}^{-3}$, $u_* = 3 \text{ cm s}^{-1}$, and $U_b/u_* = 10$. The reference position is at $z_{n,b} = 0.01$. Different α values and Reynolds numbers ($Re_* = u_*H/\nu$) are featured to illustrate overall sensitivity of the normalized SSC profile to these parameters. The Prandtl and Rouse model predictions of SSC are shown for reference in the top-left panel. The Reynolds number is varied by altering ν .

 $z_n \to 1$. The peak $(\sigma_w/u_*)^2 = 1.9$ is compatible with near-neutral atmospheric surface layer measurements (= 1.8) where lateral confinements of the flow are absent (unlike flumes and wind tunnels) and where H/η far exceeds those obtained in laboratory studies.

Now the comparisons of the CSB results in Section 3.1 with α temporarily set as a free parameter with (a) Prandtl's power law solution and (b) Rouse's formula are shown in Figure 3.

The computed SSC and Sc profiles are also presented when the flow conditions and sediment properties are provided. For Prandtl's power-law and Rouse's formula, the bulk Schmidt number was set to unity. However, the CSB model allows for a depth-dependent $Sc(z_n)$, which is set by α . When $\alpha = 0$, $Sc(z_n) = 1$ in the entire channel, consistent with Equation 28. When $\alpha > 0$, $Sc(z_n)$ varies with depth and is generally greater in the near-bed region and becomes smaller with increasing z_n . However, because of the imposition of a finite ϵ near the water surface $(=0.001\epsilon_h)$, $Sc(z_n)$ increases back to near unity when $z_n \to 1$. Rouse's equation and CSB models exhibit different behavior near the water surface. Rouse's equation yields a zero-concentration at $z_n = 1$ whereas the CSB model does not. One advantage to the CSB approach is its ability to resolve the dependence of $\overline{C}/\overline{C_b}$ on Reynolds number. Using different ν , variations in $Re_* = u_* H/\nu$ can be generated and their effects on CSB model predictions tracked. Recall that H/η_b (modeled in the CSB) scales as $Re_*^{3/4}$, and the effects of this scale separation on the shape of the vertical velocity spectrum, sediment flux co-spectrum, and the resulting $\overline{C}/\overline{C_b}$ profiles are explicitly determined. The effects of α are much more significant than the effects of Re_* , which is heuristically supportive for using Direct Numerical Simulation runs (lower Re*) to further explore the CSB approach. As earlier noted, the implications of setting $t_{wc} = \min(t_{ww}, f_o t_{K,b})$ with $f_o = \sqrt{1000}$ are most visible on the $Sc(z_n)$ profile near the free water interface. Altering f_0 primarily modifies the thickness of the region near the water interface impacted by the imposed finite t_{wc} (or finite ϵ in the Sc(k) determination). However, the CSB model itself is not expected to be valid in this zone as the assumed shape of $E_{var}(k)$ is not realistic, the flux transport terms can be finite, and turbo-phoretic effects may also be large in this vicinity. In sum, predictions from the CSB model near the free water surface must be treated with skepticism and caution.

LI ET AL. 11 of 19

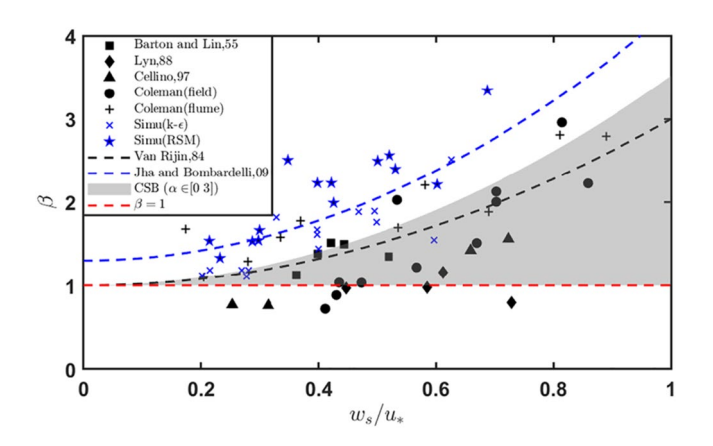


Figure 4. The model coefficient β based on different formulae, experiments, and model runs. The experiments and model runs presented here are described elsewhere (Jha & Bombardelli, 2009).

3.2. Recovery of the Rouse and Prandtl Equations

Whether a Rouse equation can be recovered from the CSB model under certain simplifications is now examined. Any explicit model must include Sc and approximations to Equation 42. Assuming $k_c/k_o \rightarrow 0$ and $k_o/k_e \rightarrow 0$ in $\Omega(z_n)$ only (i.e., setting the area under the Saffman spectrum to zero that is then partially compensated for by extending the inertial subrange to $k_e \rightarrow \infty$), the Schmidt number derived from Equation 42 can be approximated as

$$Sc^{-1} \approx 1 + B_{\pi} \left(\frac{w_s}{u_*}\right)^2$$
, with $B_{\pi} = \frac{\sqrt{15A_{\pi}}}{3C_o} \alpha \approx 0.84\alpha$, (43)

which directly recovers the quadratic model for Sc^{-1} reported elsewhere (Bombardelli & Moreno, 2012; van Rijn, 1984) as expected. With $R \approx 0$, Equation 43 indicate $\beta = Sc^{-1} \rightarrow 1$ thereby recovering Rouse's original assumption (i.e., SS resemble passive scalars in this case). This estimate of β also allows for the determination of the model coefficient α using a separate data set and model runs shown in Figure 4.

Figure 4 shows different predictions of β , including $\beta = 1 + 2(w_s/u_*)^2$ (van Rijn, 1984) and $\beta = 1.3 + 3(w_s/u_*)^2$ (Jha & Bombardelli, 2009) for model

results that explicitly consider particle-fluid interactions. Moreover, with Sc provided in Equation 43, the SS diffusivity is derived as,

$$\frac{D_s(z)}{\kappa z u_*} = \frac{1}{Sc} (1 - z_n) = \left[1 + B_\pi \left(\frac{w_s}{u_*} \right)^2 \right] (1 - z_n)$$
 (44)

where $\kappa_z u_*$ is the eddy viscosity in the log-region of $\overline{u}(z)$. Depending on choices made for α or B_π , a number of empirical relations can be recovered including the widely used Rouse's equation and variants on it (Hunt, 1954). For a given α , an analytical solution for the SSC can be derived and compared with published experiments. The SSC solution for an arbitrary α is given as

$$\frac{\overline{C}(z_n)}{\overline{C}_h} = \left(\frac{z_n}{1 - z_n} \frac{1 - z_{n,b}}{z_{n,b}}\right)^{-R_+}.$$
(45)

Where the power exponent R_{\perp} is defined as

$$R_{+} = \frac{1}{1 + B_{-}(w_{c}/u_{*})^{2}} \frac{w_{s}}{\kappa u_{*}}.$$
 (46)

When $\alpha=0$ (or $B_\pi=0$), a quadratic diffusivity profile (O'Brien, 1933) as well as Rouse's formula (Rouse, 1937, 1939) for SSC given in Equation 16 are recovered. Furthermore, in the limit of $(z_n\ll 1)$ a linear diffusivity profile (von Karman, 1934) along with the classic power law solution are also recovered from Equation 45. The consequences on σ_w^2 of setting the Saffman spectrum to zero and extending the inertial subrange to $k\to\infty$ on σ_w^2 are briefly discussed using Figure 2. As expected, these approximation over-estimate $(\sigma_w/u_*)^2$ in the near-wall region and underestimate $(\sigma_w/u_*)^2$ in the outer layer when compared to a $E_{ww}(k)$ that accommodates the Saffman spectrum (i.e., large scale effects) but truncates the inertial subrange at $1/k_e$. These effects cannot be readily ignored and may influence the choices made about α .

3.3. Comparison With Experiments

The CSB model given by Equations 40 and 38 and its simplified version featured in Equation 45 are compared with published experiments (Greimann & Holly, 2001; Tseng & Tinoco, 2020; Vanoni, 1984) summarized in Table 1. We assume $\Phi(z) = 0$ thereby neglecting inertial effects for compatibility with operational models (e.g., the Rouse model). The comparisons with published experiments are shown in Figure 5. For these experiments, all

LI ET AL. 12 of 19



Table 1 Summary of Published Experiments and Parameters Used in Model-Data Comparisons						
Run	(a)	(b)	(c)	(d)	(e)	(f)
Flow properties						
$H\left(\mathbf{m}\right)$	0.10	0.52	0.50	0.10	0.10	0.10
<i>B</i> (m)	_	0.84	0.84	0.15	0.15	0.15
U_b (measured, m s ⁻¹)	1.98	3.95	3.63	0.31	0.22	0.17
$Re_b = U_b H/\nu \times 10^{-4}$	18.7	193	170	2.9	2.1	1.6
$Re_{pa} = u_* d_s / \nu$	103	169	166	16	13	7
$u_* \text{ (cm s}^{-1}\text{)}$	7.67	20.0	20.0	1.7	1.4	0.8
$z_{n,b} \times 10^2$ (measured)	6.3	2.6	3.0	5.0	3.8	5.6
$z_{n,b}^+ \left(= u_* z_b / \nu\right)$	456	2,747	2,988	85	53	45
U_b/u_* (measured)	25.8	19.4	18.2	18.2	15.7	21.3
Sediment properties						
$\rho_s I \rho$	1.05	2.65	2.65	1.20	1.20	1.20
d_s (mm)	1.42	0.88	0.88	1.00	1.00	1.00
w_s (cm s ⁻¹)	1.7	10	10	2.9	2.9	2.9
Dimensionless model parameters						
$R_* = w_s / (\kappa u_*)$	0.5	1.2	1.2	4.3	5.2	9.1
α	27.7	14.5	16.3	0.6	0.4	0.2
β (Rouse)	1.3	1.6	1.8	2.2	2.2	2.8
$R = w_s / (\beta \kappa u_*)$	0.4	0.8	0.7	1.9	2.4	3.2
β (Prandtl)	0.9	1.1	1.2	1.4	1.5	1.9
$R = w_s / (\beta \kappa u_*)$	0.6	1.1	1.0	3.0	3.5	4.8
$St_b\left(=w_s/g\sqrt{gS_oU_b/\nu}\right)$	0.57	5.63	5.4	0.09	0.06	0.03
$St_+ \left(= \tau_p u_* / H\right) \times 10^3$	1.3	4.0	4.1	0.5	0.4	0.2
$Fr_d \left(= U_b / \sqrt{(\rho_s / \rho - 1) g d_s}\right)$	75	33	30	7	5	4
Fr_{dc}	3	4	4	3	3	3
U_b/u_* (CSB rough bed)	12.4	15.2	15.6	13.0	14.0	13.5
U_b/u_* (CSB smooth bed)	27.2	33.1	33.5	23.5	23.7	22.4

Note. When setting Sc=1, not all runs are classified as SS (or $0.8 \le R_* \le 2.5$) even though sediments were reported as suspended. While St_b is not very small for (b) and (c), $St_+ \ll 1$. Calculated densimetric and critical Froude numbers (Fr_d and Fr_{dc}) are presented along with the roughness Reynolds number Re_{pa} . All experiments lie in the fully rough ($Re_{pa} > 100$) or transitional (3 < $Re_{pa} < 100$) regimes in fully developed turbulence ($Re_b \ge 500$). The ratio between the sediment diameter and the Kolmogorov length scale varies from 3 to 25 across all the measurements used here.

the reported parameters including measured u_* , d_s , and ρ_s and the fitted β (needed for assessing the fitted Rouse equation) and α (needed for evaluating the numerical CSB model) are presented in Table 1.

In the experiments, the sediments covered the bed and were assumed to have reached an equilibrium state where Equation 4 applies (Tseng & Tinoco, 2020). The densimetric Froude number Fr_d and the critical densimetric Froude number Fr_d whose formulation is described elsewhere (Ali & Dey, 2017, 2018; Li & Katul, 2019) are also presented in Table 1. In all cases, the U_b , ρ_s/ρ , and d/H result in $Fr_d > Fr_{dc}$ meaning that sediments can be released from the bed and must be balanced by sediments depositing onto the bed. Thus, the experiments here do not strictly abide by H.A. Einstein's definition of SS as sediments cannot remain permanently suspended. Across the experiments, the flow variables U_b and u_* varied from 10 cm s⁻¹ to 40 cm s⁻¹ and 0.8–8 cm s⁻¹, respectively. However, $U_b/u_* = (8/f_{dw})^{1/2}$, related to the Darcy-Weisbach friction factor f_{dw} , varied much less (15–25) as may be anticipated in fully rough flow over a channel bed covered by grains of similar d_* . The particle properties ρ_*/ρ

LI ET AL. 13 of 19



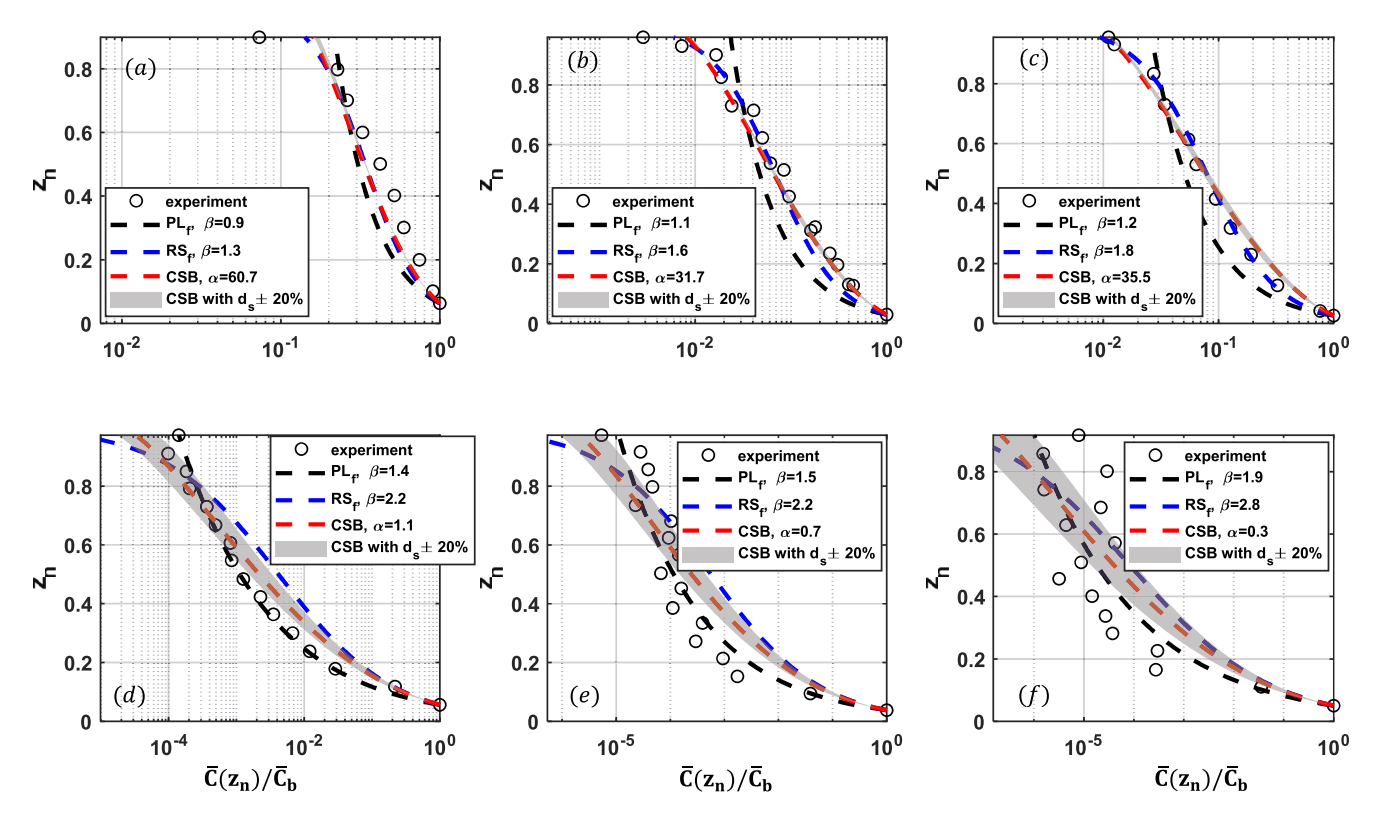


Figure 5. The predicted suspended sediment concentration profiles normalized by C_b selected at the measurement height with the highest reported concentration. The panel labeling follows Table 1 with the top panel showing the comparisons from earlier measurement that is, (a) (Greimann & Holly, 2001; Wang & Qian, 1992) and (b)–(c) (Vanoni, 1984), and the bottom panel showing the comparisons using recent experiments (d)–(f) (Tseng & Tinoco, 2020). For experiments in panels (a)–(c), the St_b is not small (>0.5).

and d_s varied from 1.05 to 2.65 and 0.88–1.4 mm, respectively. The consequence of these variations is that the empirically derived settling velocity w_s is much smaller than the Stokes settling velocity as shown in the inset of Figure 1. Collectively, these experiments span wide-ranging particle sizes (in the SS range) and flow properties from different sources. The lowest measured sediment concentration near the channel bottom is close to the surface ($z_{n,b} \in [0.026, 0.063]$) but remains above the buffer region $z^+ = u_* z_b / \nu > 30$ as shown in Table 1. For some runs, the $z^+ < 100$ and wall-blockage effects (not considered here) can impact $E_{ww}(k)$ and $d\bar{u}(z)/dz$ (McColl et al., 2016), which introduce obvious uncertainties. As shown in Table 1, experiments (a)-(c) are characterized by $St_b > 0.5$, which may be indicative that $\Phi(z)$ is not small. Experiments (d)-(f) are characterized by a small St_b as assumed by the CSB and Rouse's formula.

Figure 5 confirms that the fitted Rouse formula and fitted Prandtl formula (i.e., the R model, allowing β to be fitted) offer good agreements with some measurements (for (a)-(b) and (d)-(f) respectively) at all depths. Given that the simplified CSB model is identical to Rouse's formula, an agreement between the fitted Rouses's formula and the measurements can also be juxtaposed to the simplified CSB model. However, the numerical CSB model provides reasonable agreements for all the runs when allowing α to vary. Allowing α to be a free parameter has several advantages when compared to β in the fitted Rouse equation. Setting β as constant implies Sc is constant at all z_n while setting α as constant incorporates some of the local variations in Sc with z_n (albeit near the free water surface, maintaining a finite ϵ can be problematic without adjustments). The impact of minor variations in particle sizes is shown in the shaded area: the particle sizes are increased/decreased by 20% to illustrate model sensitivity to d_s . Uncertainty in sediment composition (and thus d_s and w_s) can be a factor in determining SSC uncertainty but not in all cases (runs d–f). While the SSC model does not require \overline{u} (only $d\overline{u}/dz$), the predicted U_b from the CSB turbulent stress budget can be compared against measured U_b for a plausibility check. The modeled U_b requires u_* along with a boundary condition specified here as \overline{u} ($z_{n,b}$) / u_* at $z_{n,b}$. A number of choices can be made about this boundary condition. Given that $z_{n,b}$ is sufficiently distant from the wall, the most direct of

LI ET AL. 14 of 19

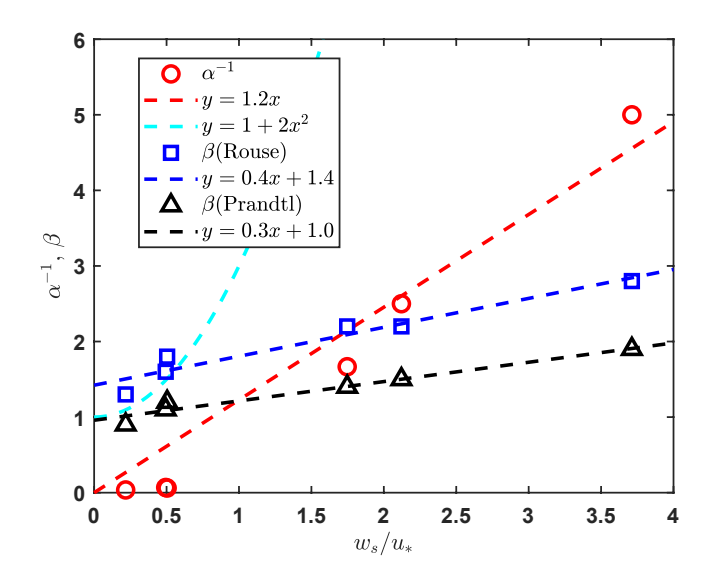


Figure 6. The dependence of fitted α and β on the w_s/u_* . The red, blue and black dashed lines show the fitted trend-lines of α^{-1} and β from Rouse and Prandtl equations respectively. The cyan dashed line is $\beta = 1 + 2(w_s/u_*)^2$ (van Rijn, 1984) extrapolated for large w_s/u_* .

those choices is the log-law for two end-member cases: (a) fully rough with an externally imposed surface roughness and (b) hydrodynamically smooth. In both cases, the mean velocity at $z_{n,h}$ is approximated as

$$\frac{\overline{u}(z_b)}{u_*} = \frac{1}{\kappa} \log\left(\frac{z_b}{z_o}\right); \qquad \frac{\overline{u}(z_b)}{u_*} = \frac{1}{\kappa} \ln\left(z_{n,b}^+\right) + 5,\tag{47}$$

where z_o is the momentum roughness length. The z_o can be related to d_s by $z_o \approx d_s/30$ where the grain diameter is assumed constant. In all cases, the particle roughness Reynolds number $Re_{pa} = u_*d_s/\nu > 3$ but in some cases, the flow is not fully rough (i.e., transitional with $3 < Re_{pa} < 100$). For this reason, the CSB model forced by both rough and smooth surface boundary conditions at $z_{n,b}$ are featured in Table 1. The agreement between measured and the range of CSB modeled U_b/u_* for these two end-member cases appears reasonable. Runs (a) and (f) are closer to a smooth-wall case whereas runs (b), (c), and (e) are better approximated by a rough-wall boundary condition. Run (d) falls in-between these two end-member cases. While Run (f) had the smallest $Re_{pa} = 8$ and a near-smooth wall approximation may be justifiable, run (a) had a $Re_{pa} > 100$. We do not have a clear explanation as to why U_b in run (a) is better approximated by a smooth wall boundary condition.

An investigation of the relation between fitted α (and β) and w_s/u_* is undertaken and shown in Figure 6. A near-linear relation between α^{-1} and w_s/u_* indirectly supports the heuristic closure adopted for $\overline{C'\partial w'/\partial z}$ with some caveats

In the regime $w_s/u_*\gg 1$, the closure model with $b_1\sim \mathrm{sgn}(A_f)u_*/w_s$ leads to an $\alpha^{-1}\sim -\mathrm{sgn}(A_f)(1-C_I)(w_s/u_*)$ and $\beta\sim -\mathrm{sgn}(A_f)/(1-C_I)(w_s/u_*)$, both of which are negative unless $\mathrm{sgn}(A_f)$ is negative. The relation in Figure 6 indicates a positive slope between fitted α^{-1} and w_s/u_* , suggesting that the coefficient A_f in the flux-variance similarity closure (i.e., Equation 22) is negative. More broadly, to what extent this closure is general and how robust are its results in the context of SSC profile predictions cannot be unpacked from the experiments here and is better kept for a future research topic.

4. Model Limitations

The treatment of suspended sediments as a dilute mixture is an obvious model limitation. This assumption requires particles to settle independently and that the solid volume can be ignored relative to the water volume. For the experiments considered here, this assumption is reasonable. Another restrictive assumption is setting $\Phi = 0$ (Chamecki et al., 2007; Kind, 1992). A $\Phi = 0$ also leads to $\overline{C} = \overline{w'C'}/w_s \to 0$ at $z_n \to 1$, which may not be general. Given the large vertical gradients in σ_w^2 near the channel bottom and near the free water surface, turbophoretic effects can be significant in these two regions (Caporaloni et al., 1975; Chamecki et al., 2007; Guha, 1997; Katul et al., 2010; Marchioli & Soldati 2002; Zhao & Wu, 2006). The turbophoretic effect act to increase the SS concentration near the water surface; however, the measurements here (runs a-c) suggest that for the $St_b > 1$ cases, the SS concentrations near the water surface experience a decline as $z_n \to 1$ instead of an increase. This finding can be used to suggest that $\Phi = 0$ may be plausible as the turbophoretic term was shown to dominate Φ near the water surface (Bragg et al., 2021; Richter & Chamecki, 2018). The CSB budget formulation here (i.e., Equation 32) ignored the flux transfer term and their vertical variation. In the case of the turbulent stress, ignoring the flux transfer term (and its vertical gradients) altogether guarantees that the co-spectrum between w' and u' in the inertial subrange maintains a $k^{-7/3}$ scaling. This $k^{-7/3}$ scaling has been observed in numerous boundary layer studies reporting co-spectra thereby offering indirect justification for this assumption. The flux transport terms (i.e., the vertical gradients of triple moments in the Reynolds averaged equations) have also been ignored. These terms have been studied less for stress and sediment flux turbulent budgets compared to their turbulent kinetic energy budget counterparts. The work here highlights the need for an assessment of these terms relative to their mechanical production terms. The CSB model also assumes that the linear Rotta scheme (slow component) with an isotropization of production (rapid component) applies equally to SS and momentum

LI ET AL. 15 of 19



fluxes without adjustments in constants (i.e., $A_R = 1.8$ and $C_I = 3/5$). Hence, any departure from these established constants must be absorbed by $t_{\text{new}}(k)/t_r(k)$, which manifests itself as a Schmidt number effect (or α variations).

The assumed shape of $E_{uv}(k)$ is also over-simplified and certainly not reflective of what is known about the energetics near the surface $(z^+ < 100)$ such as wall-blockage. Moving away from the wall region itself, other 'shape issues' arise. For example, near the spectral transition from inertial to viscous regimes, usually occurring at around $k\eta \approx 0.1$, $E_{\text{num}}(k)$ experiences a bottleneck that is absent here (Katul et al., 2015; Saddoughi & Veeravalli, 1994). Likewise, as $k\eta > 0.1$ and increases further into the viscous regime, $E_{ww}(k)$ decays exponentially (Pope, 2000). Hence, extending the inertial subrange to $k\eta = 1$ is not intended to capture all such mechanisms impacting the vertical velocity spectrum. Instead, it allows for some compensation of loss in energy due to censoring $E_{uu}(k)$ at $k\eta = 1$ while introducing extra energy due to an expected overestimation of the extrapolated inertial subrange spectrum in this vicinity. On a more positive note, while the full details of the turbulent kinetic energy cascade across scales are not explicitly considered, their effects remain implicitly contained in the assumed shape of $E_{uu}(k)$. As such, some of these effects can be accommodated (e.g., the bottleneck, viscous cutoff, etc...) by various revisions to $E_{uuv}(k)$ (e.g., including a bump around $k\eta = 0.1$, resolving the viscous cutoff region using the Pao spectral shape or variants (Pope, 2000) on it, etc...). The co-spectral budget is integrated scale-wise, which means that the precise shape of $E_{ww}(k)$ in the vicinity of $k\eta \approx 1$ is less crucial. Moving beyond the shape issues of $E_{unu}(k)$ and focusing on its primary input variable $\epsilon(z_n)$, the approach assumes turbulent kinetic energy production is balanced by its dissipation at every z_n (i.e., $\phi(z_n) = 1$), which is certainly not realistic for all z_n . However, as previously mentioned, deviations from unity in $\phi(z_n)$ may be ameliorated by the sub-unity exponent (-1/3) dependence in the SSC budget. An exception to this statement is the particle time scale $t_{w}(k)$ in Sc(k). A $\phi(z_n) = 1$ as $z_n \to 1$ leads to an unbounded $Sc^{-1}(k)$ and thus an uncertain D_s shape in the vicinity of the free surface. A plausible adjustment to the $Sc^{-1}(k)$ calculations based on maintaining a minimal ϵ (=0.001 ϵ_k) was introduced here though this correction remains ad-hoc. Last, the turbulent SS flux from the CSB model(s) follows the same form as gradient-diffusion closure upon ignoring both - turbulent flux transport and scale-wise transfer terms. However, a key advantage here is that the effective diffusion coefficient D_a from the CSB model contains contributions from turbulent eddies and Schmidt numbers at all scales. The proposed Schmidt number (or α) is consistent with bulk Schmidt number formulations such as those by van Rijin's and other one-way coupling schemes (i.e., particle transport does not impact the flow) when Sc < 1 (Bombardelli & Moreno, 2012). For dense mixture or other aeolian particles in the atmosphere, the particle Schmidt number can be larger than unity (Csanady, 1963) implying other particle-fluid interaction models are required. When using the CSB model, the α used for the determination of the Schmidt number is treated as a single fitted parameter. Hence, the CSB model offers the same number of free parameters as the fitted Rouse equation. What was found here is that α^{-1} varies linearly with w/u_* when combining all the experiments. A plausibility argument as to why α depends on w/u_* was also offered. In some instances, the addition of a single fitted parameter may be desirable in hydraulic models as discussed elsewhere (Battiato & Rubol, 2014; Li, Katul, & Huai, 2019; Papke & Battiato, 2013; Rubol et al., 2018), but an increasing number of free model parameters does not necessarily lead to a better physical understanding. The sediment settling velocity estimated in Equation 7 is commonly based on a mass-median-diameter from particle size distribution measurements, which however may not be an optimized characteristic size as shown by some in-situ measurements (Williams et al., 2007). Large variations in d, can have a substantial impact on SSC profiles, which may be more significant than models for α .

5. Conclusion

Operational modeling of SSC in turbulent flows continues to be a formidable challenge in hydraulics, hydrology, ecology, and water quality control. The work here establishes a new link between the spectrum of vertical velocity and SS turbulent flux, which was then used to arrive at expressions for the SSC profile. The spectrum of vertical velocity is characterized by multiple scaling regimes that include the Saffman spectrum $(E_{ww}(k) \sim k^{+2})$, the "energy splashing" effect due to the presence of a wall $(E_{ww}(k) \sim k^0)$, and the much-studied inertial subrange regime $(E_{ww}(k) \sim k^{-5/3})$. Finite Reynolds effects are accommodated through a scale separation between z and the Kolmogorov microscale η terminating the scale-wise extent of the inertial subrange (as a first approximation). This dependence can be noted when considering the scaling argument $k_e/k_o = z/\eta \sim (zu_*/v)^{3/4}$ (Tennekes & Lumley, 1972). Hence, increasing $Re_s = (zu_*/v)$ by either increasing z or u_* leads to a widening of the scale-wise extent of the inertial subrange, which then impacts all subsequent expressions such as $\Omega(z_n)$ and $d\bar{u}/dz$. As such,

LI ET AL. 16 of 19



Acknowledgments

SL was supported by a fellowship from

the Nicholas School of the Environment at

Duke University. GK and ADB acknowl-

Science Foundation (NSF-AGS-1644382,

NSF-AGS-2028633, NSF-IOS-1754893,

edge support from the U.S. National

and NSF-CBET-2042346).

the proposed model is responsive to finite Reynolds number, Schmidt number, and Rouse number effects. Prior ad-hoc efforts such as correcting l_0 by V_n (i.e., the van Driest damping function) can now be interpreted from this new spectral perspective (i.e., Re, effects become large for small z or u*). A simplified solution to the CSB model in which the Saffman spectrum is truncated but the inertial subrange is now extended to infinite wave-numbers (i.e., $Re_s \rightarrow \infty$) was shown to recover earlier theories (e.g., Rouse's formula). The fitted Rouse's equation (and by extension the simplified CSB solution) also describes the measured SSC profiles in all the experiments considered here provided α (or β) is allowed to vary with w_{Ju_*} . Thus, one of the main novelties here is to provide a spectral link between the energy distribution in eddies and the SSC shape. Interactions between turbulent eddies and suspended sediment grains at various heights were also proposed, resulting in a scale-dependent Sc captured by a single parameter α that varies with w_{γ}/u_{*} . Such Sc variations were formulated in spectral space but recover expected bulk relations between R and Sc identified by other models, experiments, and simulation studies. When all these findings are taken together, future extension of this work must focus on upgrading the particle-turbulence interaction scheme and its signature in a scale-dependent Schmidt number. Such extension will benefit from targeted DNS runs where all the terms in the particle co-spectrum as well as $E_{ww}(k)$ can be computed or determined. Likewise, an exploration of where the sediment flux transport term is significant relative to the mechanical production term and how to incorporate its effects can be undertaken from the aforementioned DNS runs.

Data Availability Statement

All the data used were digitized from the published literature (Greimann & Holly, 2001; Jha & Bombardelli, 2009; Tseng & Tinoco, 2020; Vanoni, 1984).

References

- Albertson, J. D., Parlange, M. B., Katul, G. G., Chu, C.-R., Stricker, H., & Tyler, S. (1995). Sensible heat flux from arid regions: A simple flux-variance method. *Water Resources Research*, 31(4), 969–973.
- Ali, S. Z., & Dey, S. (2017). Origin of the scaling laws of sediment transport. *Proceedings of the Royal Society A: Mathematical, Physical & Engineering Sciences*, 473(2197).
- Ali, S. Z., & Dey, S. (2018). Impact of phenomenological theory of turbulence on pragmatic approach to fluvial hydraulics. *Physics of Fluids*, 30(4), 045105.
- Ayet, A., & Katul, G. (2020). Scaling laws for the length scale of energy-containing eddies in a sheared and thermally stratified atmospheric surface layer. *Geophysical Research Letters*, 47(23), e2020GL089997.
- Battiato, I., & Rubol, S. (2014). Single-parameter model of vegetated aquatic flows. Water Resources Research, 50(8), 6358-6369.
- Bombardelli, F., & Jha, S. (2009). Hierarchical modeling of the dilute transport of suspended sediment in open channels. *Environmental Fluid Mechanics*, 9(2), 207.
- Bombardelli, F., & Moreno, P. (2012). Exchange at the bed sediments-water column interface (2nd ed.). In C. Gualtieri & D. T. Mihailovic (Eds.), Fluid mechanics of environmental interfaces (pp. 221–253).
- Bonetti, S., Manoli, G., Manes, C., Porporato, A., & Katul, G. (2017). Manning's formula and Strickler's scaling explained by a co-spectral budget model. *Journal of Fluid Mechanics*, 812, 1189–1212.
- model. *Journal of Fluid Mechanics*, 812, 1189–1212.

 Bos, W., Touil, H., Shao, L., & Bertoglio, J.-P. (2004). On the behavior of the velocity-scalar cross correlation spectrum in the inertial range.
- Physics of Fluids, 16(10), 3818–3823.
 Bragg, A. D., Richter, D. H., & Wang, G. (2021). Mechanisms governing the settling velocities and spatial distributions of inertial particles in
- wall-bounded turbulence. *Physical Review Fluids*, 6(6), 064302.

 Caporaloni, M., Tampieri, F., Trombetti, F., & Vittori, O. (1975). Transfer of particles in nonisotropic air turbulence. *Journal of the Atmospheric Sciences*, 32(3), 565–568.
- Castro-Orgaz, O., Giráldez, J., Mateos, L., & Dey, S. (2012). Is the Von Kármán constant affected by sediment suspension? *Journal of Geophysical Research: Earth Surface*, 117(F4).
- Cava, D., & Katul, G. (2012). On the scaling laws of the velocity-scalar cospectra in the canopy sublayer above tall forests. *Boundary-Layer*
- Meteorology, 145(2), 351–367.

 Chamecki, M., Van Hout, R., Meneveau, C., & Parlange, M. B. (2007). Concentration profiles of particles settling in the neutral and stratified atmospheric boundary layer. Boundary-Layer Meteorology, 125(1), 25–38.
- Cheng, N.-S. (1997). Simplified settling velocity formula for sediment particle. *Journal of Hydraulic Engineering*, 123(2), 149–152.
- Csanady, G. (1963). Turbulent diffusion of heavy particles in the atmosphere. Journal of the Atmospheric Sciences, 20(3), 201-208.
- Dai, Z., Fagherazzi, S., Mei, X., & Gao, J. (2016). Decline in suspended sediment concentration delivered by the Changjiang (Yangtze) River into the East China Sea between 1956 and 2013. *Geomorphology*, 268, 123–132.
- Dey, S. (2014). Fluvial hydrodynamics. Springer.
- Dey, S., & Ali, S. Z. (2020). Fluvial instabilities. Physics of Fluids, 32(6), 061301.
- Duman, T., Trakhtenbrot, A., Poggi, D., Cassiani, M., & Katul, G. G. (2016). Dissipation intermittency increases long-distance dispersal of heavy particles in the canopy sublayer. *Boundary-Layer Meteorology*, 159(1), 41–68.
- Einstein, H. (1950). The bed-load function for sediment transportation in open channel flows (No. 1026) (Technical Report). US Department of Agriculture, Soil Conservation Service.
- Elghobashi, S. (1994). On predicting particle-laden turbulent flows. Applied Scientific Research, 52(4), 309-329.
- Ferry, J., & Balachandar, S. (2001). A fast Eulerian method for disperse two-phase flow. *International Journal of Multiphase Flow*, 27(7), 1199–1226.

LI ET AL. 17 of 19



- Fischer, H. B., List, J. E., Koh, C. R., Imberger, J., & Brooks, N. H. (2013). Mixing in inland and coastal waters. Elsevier.
- Giometto, M., Katul, G., Fang, J., & Parlange, M. (2017). Direct numerical simulation of turbulent slope flows up to Grashof number $Gr = 2.1 \times 10^{11}$. Journal of Fluid Mechanics, 829, 589.
- Green, M., & Coco, G. (2014). Review of wave-driven sediment resuspension and transport in estuaries. Reviews of Geophysics, 52(1), 77-117.
- Greimann, B., & Holly, F., Jr. (2001). Two-phase flow analysis of concentration profiles. *Journal of Hydraulic Engineering*, 127(9), 753–762.
- Greimann, B., Muste, M., & Holly, F., Jr. (1999). Two-phase formulation of suspended sediment transport. *Journal of Hydraulic Research*, 37(4), 479–500
- Guha, A. (1997). A unified Eulerian theory of turbulent deposition to smooth and rough surfaces. *Journal of Aerosol Science*, 28(8), 1517–1537.
 Heisel, M., Katul, G., Chamecki, M., & Guala, M. (2020). Velocity asymmetry and turbulent transport closure in smooth-and rough-wall boundary layers. *Physical Review Fluids*, 5(10), 104605.
- Huai, W., Yang, L., & Guo, Y. (2020). Analytical solution of suspended sediment concentration profile: Relevance of dispersive flow term in vegetated channels. Water Resources Research, 56(7), e2019WR027012.
- Huai, W., Yang, L., Wang, W.-J., Guo, Y., Wang, T., & Cheng, Y.-g. (2019). Predicting the vertical low suspended sediment concentration in vegetated flow using a random displacement model. *Journal of Hydrology*, 578, 124101.
- Huai, W.-x., Li, S., Katul, G. G., Liu, M.-y., & Yang, Z.-h. (2021). Flow dynamics and sediment transport in vegetated rivers: A review. *Journal of Hydrodynamics*, 33(3), 400–420.
- Huang, C.-W., Launiainen, S., Grönholm, T., & Katul, G. G. (2014). Particle deposition to forests: An alternative to K-theory. Atmospheric Environment. 94, 593–605.
- Hunt, J. (1954). The turbulent transport of suspended sediment in open channels. Proceedings of the Royal Society of London Series A: Mathematical and Physical Sciences, 224(1158), 322–335.
- Jha, S. K., & Bombardelli, F. A. (2009). Two-phase modeling of turbulence in dilute sediment-laden, open-channel flows. *Environmental Fluid Mechanics*, 9(2), 237.
- Johnson, P. L., Bassenne, M., & Moin, P. (2020). Turbophoresis of small inertial particles: Theoretical considerations and application to wall-modelled large-eddy simulations. *Journal of Fluid Mechanics*, 883, A27. https://doi.org/10.1017/jfm.2019.865
- Katul, G. G., Grönholm, T., Launiainen, S., & Vesala, T. (2010). Predicting the dry deposition of aerosol-sized particles using layer-resolved canopy and pipe flow analogy models: Role of turbophoresis. *Journal of Geophysical Research: Atmospheres*, 115(D12).
- Katul, G. G., & Manes, C. (2014). Cospectral budget of turbulence explains the bulk properties of smooth pipe flow. *Physical Review E*, 90(6),
- Katul, G. G., Manes, C., Porporato, A., Bou-Zeid, E., & Chamecki, M. (2015). Bottlenecks in turbulent kinetic energy spectra predicted from structure function inflections using the von Kármán-Howarth equation. *Physical Review E*, 92(3), 033009.
- Katul, G. G., Porporato, A., Manes, C., & Meneveau, C. (2013). Co-spectrum and mean velocity in turbulent boundary layers. *Physics of Fluids*, 25(9), 091702.
- Kellogg, M. L., Smyth, A. R., Luckenbach, M. W., Carmichael, R. H., Brown, B. L., Cornwell, J. C., & Higgins, C. B. (2014). Use of oysters to mitigate eutrophication in coastal waters. Estuarine. Coastal and Shelf Science, 151, 156–168.
- Kim, J., Moin, P., & Moser, R. (1987). Turbulence statistics in fully developed channel flow at low Reynolds number. *Journal of Fluid Mechanics*, 177, 133–166.
- Kind, R. (1992). One-dimensional aeolian suspension above beds of loose particles—A new concentration-profile equation. Atmospheric Environment Part A. General Topics, 26(5), 927–931.
- Li, D., Katul, G. G., & Zilitinkevich, S. S. (2015). Revisiting the turbulent Prandtl number in an idealized atmospheric surface layer. *Journal of the Atmospheric Sciences*, 72(6), 2394–2410.
- Li, S., & Katul, G. (2019). Cospectral budget model describes incipient sediment motion in turbulent flows. Physical Review Fluids, 4(9), 093801.
- Li, S., & Katul, G. (2020). Contaminant removal efficiency of floating treatment wetlands. Environmental Research Letters, 15(10), 1040b7.
- Li, S., & Katul, G. (2021). Roughness-induced critical phenomenon analogy for turbulent friction factor explained by a co-spectral budget model. *Physics of Fluids*, 33(10), 105127.
- Li, S., Katul, G., & Huai, W. (2019). Mean velocity and shear stress distribution in floating treatment wetlands: An analytical study. Water Resources Research, 55(8), 6436–6449.
- Li, Y., Wang, X., Fu, W., Xia, X., Liu, C., Min, J., et al. (2019). Interactions between nano/micro plastics and suspended sediment in water: Implications on aggregation and settling. Water Research, 161, 486–495.
- Liu, T., Xia, X., Liu, S., Mou, X., & Qiu, Y. (2013). Acceleration of denitrification in turbid rivers due to denitrification occurring on suspended sediment in oxic waters. *Environmental Science and Technology*, 47(9), 4053–4061.
- Long, C. M., & Pavelsky, T. M. (2013). Remote sensing of suspended sediment concentration and hydrologic connectivity in a complex wetland environment. *Remote Sensing of Environment*, 129, 197–209.
- Lupker, M., France-Lanord, C., Lavé, J., Bouchez, J., Galy, V., Métivier, F., & Mugnier, J. (2011). A Rouse-based method to integrate the chemical composition of river sediments: Application to the Ganga basin. *Journal of Geophysical Research: Earth Surface*, 116(F4).
- Marchioli, C., & Soldati, A. (2002). Mechanisms for particle transfer and segregation in a turbulent boundary layer. *Journal of Fluid Mechanics*,
- 468, 283.

 Mazumder, B., & Ghoshal, K. (2006). Velocity and concentration profiles in uniform sediment-laden flow. Applied Mathematical Modelling,
- 30(2), 164–176.

 McColl, K., Katul, G., Gentine, P., & Entekhabi, D. (2016). Mean-velocity profile of smooth channel flow explained by a cospectral budget model
- with wall-blockage. *Physics of Fluids*, 28(3), 035107.

 Mohtar, W. H. M. W., Lee, J. W., Azha, N. I. M., & Cheng, N.-S. (2020). Incipient sediment motion based on turbulent fluctuations. *International*
- Journal of Sediment Research, 35(2), 125–133.

 Muste, M., Yu, K., Fujita, I., & Ettema, R. (2005). Two-phase versus mixed-flow perspective on suspended sediment transport in turbulent chan-
- nel flows. Water Resources Research, 41(10).

 Nazeer, S., Hashmi, M. Z., & Malik, R. N. (2014). Heavy metals distribution, risk assessment and water quality characterization by water quality
- index of the River Soan, Pakistan. Ecological Indicators, 43, 262–270.
- Nezu, I., & Azuma, R. (2004). Turbulence characteristics and interaction between particles and fluid in particle-laden open channel flows. *Journal of Hydraulic Engineering*, 130(10), 988–1001.
- Nie, S., Sun, H., Zhang, Y., Chen, D., Chen, W., Chen, L., & Schaefer, S. (2017). Vertical distribution of suspended sediment under steady flow: Existing theories and fractional derivative model. *Discrete Dynamics in Nature and Society*, 5481531.
- Nikora, V. I., & Goring, D. G. (2002). Fluctuations of suspended sediment concentration and turbulent sediment fluxes in an open-channel flow. Journal of Hydraulic Engineering, 128(2), 214–224.

LI ET AL. 18 of 19



- O'Brien, M. (1933). Review of the theory of turbulent flow and its relation to sediment-transportation. *EOS Transactions American Geophysical Union*, 14(1), 487–491.
- Papke, A., & Battiato, I. (2013). A reduced complexity model for dynamic similarity in obstructed shear flows. *Geophysical Research Letters*, 40(15), 3888–3892.
- Pope, S. (2000). Turbulent flows. Cambridge University Press.
- Raupach, M. (1981). Conditional statistics of Reynolds stress in rough-wall and smooth-wall turbulent boundary layers. *Journal of Fluid Mechanics*, 108, 363–382.
- Reeks, M. (1983). The transport of discrete particles in inhomogeneous turbulence. *Journal of Aerosol Science*, 14(6), 729–739. https://doi.org/10.1016/0021-8502(83)90055-1
- Richter, D., & Chamecki, M. (2018). Inertial effects on the vertical transport of suspended particles in a turbulent boundary layer. *Boundary-Layer Meteorology*, 167(2), 235–256.
- Rouse, H. (1937). Modern conceptions of the mechanics of fluid turbulence. *Transactions of the American Society of Civil Engineers*, 102(1), 463–505.
- Rouse, H. (1939). An analysis of sediment transportation in the light of fluid turbulence (pp. 1–40). United States Department of Agriculture. SCS-TP-25.
- Rubol, S., Ling, B., & Battiato, I. (2018). Universal scaling-law for flow resistance over canopies with complex morphology. Scientific Reports,
- Saddough, S. G., & Veeravalli, S. V. (1994). Local isotropy in turbulent boundary layers at high Reynolds number. *Journal of Fluid Mechanics*,
- 268, 333–372.

 Sardina, G., Schlatter, P., Brandt, L., Picano, F., & Casciola, C. M. (2012). Wall accumulation and spatial localization in particle-laden wall flows.
- Journal of Fluid Mechanics, 699, 50–78.

 Scully, M. E., & Friedrichs, C. T. (2003). The influence of asymmetries in overlying stratification on near-bed turbulence and sediment suspen-
- sion in a partially mixed estuary. *Ocean Dynamics*, 53(3), 208–219. Sun, L., Qiu, H., Wu, C., Niu, J., & Hu, B. X. (2020). A review of applications of fractional advection–dispersion equations for anomalous solute
- transport in surface and subsurface water. Wiley Interdisciplinary Reviews: Water, 7(4), e1448.

 Tan, G., Fang, H., Dey, S., & Wu, W. (2018). Rui-Jin Zhang's research on sediment transport. Journal of Hydraulic Engineering, 144(6),
- Tan, G., Fang, H., Dey, S., & Wu, W. (2018). Rui-Jin Zhang's research on sediment transport. *Journal of Hydraulic Engineering*, 144(6), 02518002.
- Tennekes, H., & Lumley, J. (1972). A first course in turbulence. MIT Press.
- Tseng, C., & Tinoco, R. (2020). A two-layer turbulence-based model to predict suspended sediment concentration in flows with aquatic vegetation. *Geophysical Research Letters*, e2020GL091255.
- Umeyaina, M. (1992). Vertical distribution of suspended sediment in uniform open-channel flow. *Journal of Hydraulic Engineering*, 118(6), 936–941
- Van Driest, E. (1956). On turbulent flow near a wall. Journal of the Aeronautical Sciences, 23(11), 1007–1011.
- Vanoni, V. A. (1984). Fifty years of sedimentation. Journal of Hydraulic Engineering, 110(8), 1021–1057.
- van Rijn, L. C. (1984). Sediment transport, part ii: Suspended load transport. Journal of Hydraulic Engineering, 110(11), 1613-1641.
- von Karman, T. (1934). Some aspects of the turbulence problem. In *Proceedings of the Fourth International Congress of Applied mechanics, Cambridge, England* (pp. 54–91).
- Wallin, S., & Johansson, A. (2000). An explicit algebraic Reynolds stress model for incompressible and compressible turbulent flows. *Journal of Fluid Mechanics*, 403, 89–132.
- Wang, X., & Qian, N. (1992). Velocity profiles of sediment-laden flow. *International Journal of Sediment Research*, 7(1), 27—58.
- Wells, M., & Stock, D. (1983). The effects of crossing trajectories on the dispersion of particles in a turbulent flow. *Journal of Fluid Mechanics*, 136, 31–62.
- Williams, N., Walling, D., & Leeks, G. (2007). High temporal resolution in situ measurement of the effective particle size characteristics of fluvial suspended sediment. Water Research, 41(5), 1081–1093.
- Yujun, Y., Zhaoyin, W., Zhang, K., Guoan, Y., & Xuehua, D. (2008). Sediment pollution and its effect on fish through food chain in the Yangtze river. *International Journal of Sediment Research*, 23(4), 338–347.
- Zhao, B., & Wu, J. (2006). Modeling particle deposition from fully developed turbulent flow in ventilation duct. Atmospheric Environment, 40(3), 457–466.

LI ET AL. 19 of 19